

# The core of the Canis Major galaxy as traced by Red Clump stars

M. Bellazzini<sup>1\*</sup>, R. Ibata<sup>2</sup>, N. Martin<sup>2</sup>, G.F. Lewis<sup>3</sup>, B. Conn<sup>3</sup>, M.J. Irwin<sup>4</sup>

<sup>1</sup> *INAF - Osservatorio Astronomico di Bologna, via Ranzani 1, 40127, Bologna, Italy*

<sup>2</sup> *Observatoire de Strasbourg, 11, rue de l'Université, F-67000, Strasbourg, France*

<sup>3</sup> *Institute of Astronomy, School of Physics, A29, University of Sydney, NSW 2006, Australia*

<sup>4</sup> *Institute of Astronomy, Madingley Road, Cambridge, CB3 0HA, U.K.*

7 February 2020

## ABSTRACT

The recently-discovered stellar system in Canis Major is analysed using He-burning Red Clump stars as tracers. We find that the main body of the system has an integrated absolute magnitude  $M_V = -14.1 \pm 0.9$ , a central surface brightness  $\mu_{V,0} = 24.0 \pm 0.7$  and a line-of-sight profile peaked at  $D_{\odot} = 7.2 \pm 1.0$  kpc with Half Width at Half Maximum  $\sim 2.0$  kpc, in excellent agreement with the results obtained with widely different tracers (M giants and Main Sequence stars) in previous analyses. The mean distance to the main body of Canis Major is observed to increase with increasing Galactic longitude, from  $D_{\odot} \simeq 6.3$  kpc at  $l \simeq 225^\circ$ , to  $D_{\odot} \simeq 9.3$  kpc at  $l \simeq 265^\circ$ , in good agreement with the predictions of our more recent N-body simulation that models CMa as a dwarf galaxy being accreted in a planar orbit onto the disc of the Milky Way. We confirm that the Canis Major system has all the characteristics of the relic of a dwarf galaxy seen in front of a large-scale overdensity that we detect all over the region of Galaxy considered in this study ( $220^\circ \leq l \leq 320^\circ$ , with a strong maximum around  $l = 290^\circ$  and  $b \gtrsim -5^\circ$ ) that is identified as the stellar component of the Galactic Warp. We also address a recent claim that Canis Major is on the outskirts of a larger ‘‘Argo’’ structure centred at  $l \simeq 290^\circ$ . Our analysis shows that the stellar populations in the latter are distributed over a very large distance range along the line of sight, and do not give rise to a narrow peak in density in this direction, contrary to what is observed in Canis Major. This suggests that the Argo structure is likely due to Galactic asymmetries such as the Warp.

**Key words:** Galaxy: structure - galaxies: dwarf - open clusters: general - open clusters: individual: Tombaugh 2, AM-2, Heffner 11

## 1 INTRODUCTION

During the last decade, it has been fully realised that the relics of the latest accretion events that contributed to the assembly of the Milky Way can be observationally identified and studied in detail (see, for example Ibata et al. 2001; Newberg et al. 2002; Majewski et al. 2003, and references therein). These findings simultaneously provide a qualitative confirmation and a new challenge for the current cosmological models in which the growth of large galaxies is driven by the process of hierarchical merger of sub-units (White & Rees 1978; White & Frenk 1991). The tidal disruption of dwarf galaxies within the Galactic potential may lead to the production of long-lived stellar

streams (as in the case of the dwarf spheroidal Sagittarius galaxy - Sgr dSph, see Ibata & Lewis 1998; Ibata et al. 2001; Ibata et al. 2002; Ivezić et al. 2000; Newberg et al. 2002; Majewski et al. 2003; Bellazzini, Ferraro & Ibata 2003a) that may reveal fundamental information about the process of disruption, the mass distribution within the Galactic halo of Dark Matter, its degree of clumpiness, etc. (see Ibata et al. 2001; Helmi 2004; Johnston, Law & Majewski 2005; Law, Johnston & Majewski 2005).

The recent discovery of a large stellar stream nearly coplanar with the Galactic disc (the Canis Major/Monoceros Ring, hereafter the Ring, for brevity Newberg et al. 2002; Yanny et al. 2003; Ibata et al. 2003; Majewski et al. 2003; Rocha-Pinto et al. 2003; Crane et al. 2003) suggests that the accretion of small stellar systems may have had a considerable rôle also in the assembly

\* E-mail: michele.bellazzini@bo.astro.it

of the disc components of the Milky Way (in particular, the Thick Disc) as envisaged by the latest detailed models of disc-galaxy formation within a cosmological context (Abadi et al. 2003a,b; Helmi et al. 2003).

In Martin et al. (2004a, hereafter Pap-I) we reported on the identification of a new stellar relic (the Canis Major dwarf galaxy, hereafter CMa) located at 7 – 8 kpc from the Sun whose approximate centre lies around  $(l; b) \sim (240^\circ; -7^\circ)$ , and that may be the progenitor of the Ring (see also Penarrubia et al. 2005). CMa was identified as a strong elliptical-shaped overdensity of M-giants by the comparison of star counts in Northern and Southern Galactic hemispheres (from the 2MASS All Sky Survey, Cutri et al. 2003). The structure was suggested to be possibly associated with some globular (but see Penarrubia et al. 2005) and open clusters (Martin et al. 2004a; Bellazzini et al. 2004; Crane et al. 2003). The relic appears to have luminosity and size similar to the Sgr dSph (Pap-I). The optical Color Magnitude Diagram (CMD) we obtained in Bellazzini et al. (2004, hereafter Pap-II) revealed a narrow and well-defined Main Sequence typical of an intermediate to old (age  $\sim 4$ –10 Gyr) and moderately metal deficient ( $[M/H] \sim -0.5$ ) stellar system; these results have been fully confirmed by the deeper CMD presented by Martinez-Delgado et al. (2005). A Blue Plume of possibly young stars or blue stragglers - also typical of dwarf spheroidal galaxies - has been detected in both optical CMDs. The first results of a large spectroscopic survey provided an estimate of the systemic radial velocity and velocity dispersion of CMa ( $V_r \simeq 110$  km/s;  $\sigma = 13.0$  km/s Martin et al. 2004b, hereafter Pap-III), while an estimate of the systemic proper motion has been obtained by Momany et al. (2004). Martin et al. (2005, hereafter Pap-IV) analysed the kinematics of more than 1400 Red Giant Branch and Red Clump stars around the centre of CMa, confirming the essence of the results of Pap-III, namely that CMa stars have a systemic velocity and a velocity dispersion quite different from what expected from Galactic disc stars at the considered distance and quite typical of Galactic dwarf satellite galaxies. Moreover they detected a clear distance - radial velocity gradient among CMa stars that can be explained as the effect of on-going tidal disruption of the stellar system. A significant refinement of the proper motion estimate was also obtained in Pap-IV. Other interesting investigations of the CMa relic, not strictly related to the present work or in a too preliminary stage to be fully useful for the analysis, can be found in Kinman, Saha & Pier (2004); Forbes, Strader & Brodie (2004); Sbordone et al. (2005); Mateu et al. (2005).

Momany et al. (2004) suggested that the CMa overdensity may be an effect of the stellar component of the Galactic Warp (Djorgovski & Sosin 1989; Yusifov 2004; López-Corredoira et al. 2002; Vig, Ghosh & Ojha 2005), whose broad southern maximum (as a South/North density asymmetry) lies in the range  $240^\circ \leq l \leq 300^\circ$  (López-Corredoira et al. 2002; Vig, Ghosh & Ojha 2005). In Pap-II and Pap-III, in particular, we showed that such a conclusion can be reached only if the distance distribution of the adopted tracers (M giants) is neglected and that CMa is in fact an additional overdensity of different nature with respect to the large scale Warp of the Galactic disc. On the other hand the disentanglement of the two structures may prove difficult, limiting our possibility to obtain a detailed

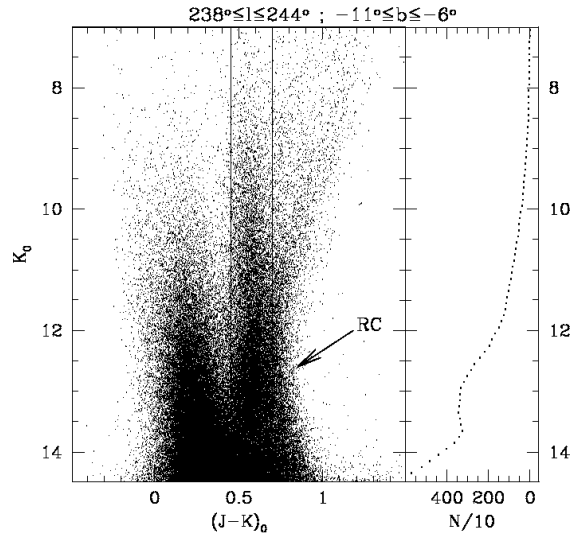


**Figure 1.** Left panel: Infrared Colour Magnitude Diagram of a  $6^\circ \times 5^\circ$  field near the centre of the CMa overdensity. The Red Clump of CMa is indicated by the arrow. The vertical lines enclose the colour range in which we select candidate RC stars. Right Panel: Luminosity Function of the selected RC stars. Note the strong bump associated with the RC of CMa at  $K \sim 13.0$ .

global description of CMa and the Warp (see Pap-III, for this discussion). A global analysis of CMa is also hampered by the large degree of contamination from Galactic stars, by the high and variable extinction toward the Galactic plane and by its proximity to us that imply a very low surface density in star counts per unit solid-angle of sky (see Sect. 4.3, below).

It is clear that a large scale study of CMa using a different tracer with respect to M-giants would provide a very useful independent check of the results of Pap-I and may help us to understand the relation between CMa and the Warp. In Pap-I we showed that the Red Clump (RC) of Helium-burning stars of the CMa system is clearly detected in the 2MASS database and in Pap-II we used the RC stars to show that CMa is an independent structure, superposed on the Galactic Warp. Here we extend the use of RC stars to trace the whole structure of the CMa relic and of the Galactic Warp in its surroundings. In Sect. 2 we describe the adopted dataset and assumptions, and we introduce our analysis method. In Sect. 3 we derive some fundamental parameters of the CMa galaxy, while in Sect. 4 we apply a technique that partially disentangles the contributions of CMa and the Warp to the global South/North asymmetry observed in the considered quadrant of the Galaxy. Finally, in Sect. 5 we summarise and discuss the main results of these analyses.

## 2 THE RED CLUMP OF CMA

We extracted from the 2MASS Point Source Catalogue the sources comprised between  $l = 220^\circ$  and  $l = 320^\circ$ , having  $-30^\circ \leq b \leq 30^\circ$ . This region of the sky was chosen

to include the main body of CMa ( $220^\circ \leq l \leq 260^\circ$  and  $-15 \lesssim b \lesssim 0$ , according to Pap-I) and the Southern maximum of the Galactic Warp. Stars were selected according to the quality of the photometry and to avoid spurious and contaminated sources as in Bellazzini et al. (2003b). The magnitudes of all the stars were corrected for extinction using the colour excesses interpolated on the COBE/DIRBE maps (Schlegel, Finkbeiner & Davis 1998) and modified according to Bonifacio, Monai & Beers (2000), as done in Momany et al. (2004) and Pap-III. The extinction laws by Rieke & Lebofsky (1985) have been adopted. In the following J, H, and K magnitudes denote reddening-corrected magnitudes  $J_0$ ,  $H_0$ , and  $K_0$ , unless otherwise stated.

In Figure 1 we show the J-K, K CMD of a low-extinction field near the centre of the CMa structure. The diagram is dominated by Main Sequence (MS) stars of the Galactic disc for  $J-K \lesssim 0.5$ , for  $J-K \gtrsim 0.8$  the M giants are contributed by both the disc and CMa, and the intermediate colour strip should be dominated by RC stars located at various distances. While the M giant sequence of CMa can be revealed only with the subtraction of a control field symmetric with respect to the Galactic Plane (Pap-I) the Red Clump of the system is clearly visible without subtraction in the range  $12 \leq K \leq 14$  with an apparent peak around  $K = 13$ , as readily shown by the histogram in the left panel of Fig. 1, in excellent agreement with Pap-I. Hence the RC feature is a very promising tracer of the CMa population. In the following we will limit our analysis to the stars in the colour strip enclosing the typical RC stars,  $0.45 \leq J - K \leq 0.75$ , as in Pap-II.

With respect to M giants, RC stars may suffer from a larger degree of contamination by unrelated sources. While for  $J - K \geq 1.0$  the only possible contaminants for M giants are M dwarfs at faint magnitudes ( $K \geq 12.0$ ), our colour-selected RC sample may be contaminated by K giants essentially at any magnitude, and both M and G dwarfs can be pushed into the RC colour range by photometric errors for  $K > 14.0$ . However all the results presented in the following are in the form of subtractions of star counts in the Southern and Northern Galactic hemispheres. Since the degree of contamination from Galactic sources as a function of magnitude should be similar in both hemispheres, the subtraction should minimise any spurious effect associated with contaminants. On the other hand RC stars should be intrinsically more numerous than M giants and they provide a completely independent and more reliable distance scale compared to the photometric parallax of M giants (see Bellazzini et al. (2003b), Majewski et al. (2003), Pap-I, Pap-II and Pap-III).

If not otherwise stated, we will use in the following only stars with  $|b| > 5.0^\circ$  to avoid the regions where the extinction is most severe (see Figs. 8 and 9, below). Note that the 2MASS Point Source Catalogue is complete down to  $K_S = 14.3$  (Cutri et al. 2003), hence the luminosity range in which the RC bump of CMa is detected  $11.5 \lesssim K \lesssim 14.2$  is not expected to suffer from problems of incompleteness.

## 2.1 Disentangling two overdensities: CMa and the Warp

It has to be noted that the origin of disc warps and the relationship between gaseous and stellar warps is far from understood (Binney 1992; Kuijken & Garcia-Ruiz 2001). More-

over the characterisation of the stellar Warp of the Milky Way is quite poor and uncertain, mainly because of the problems inherent with the analysis of stellar fields at low Galactic latitudes. Finally, it is important to realise that the adopted parametrisation may describe different characteristics of the warp and may induce some confusion in the use of terms. For instance, Djorgovski & Sosin (1989) identified the stellar warp as a sinusoidal variation of the mean latitude of their tracers (namely IRAS sources) as a function of longitude. In this case the "maximum of the warp" coincides with the maximum *angular height* above the Galactic equator, similar to the parametrisation adopted when dealing with the gaseous warp. On the other hand, López-Corredoira et al. (2002) described the warp as the sinusoidal variation of the ratio of star counts in Northern and Southern Galactic hemisphere as a function of longitude, hence their "maximum of the warp" is the region where the Southern (or Northern) overdensity reaches its maximum. The two definitions may provide very different views, depending on the structure of the disc and on the relative 3-D positions of the observed structure and the Sun. Since the CMa galaxy was identified as a South/North overdensity it should be compared with the Warp as a South/North overdensity (à la López-Corredoira et al. 2002), since this is the only relevant parameter in this context. The parametrisation of the amplitude of the Warp as the artificial shift to apply to the Galactic plane to match the star counts in the Northern and Southern hemisphere (as done by Momany et al. 2004) is not a fair description of South/North overdensities in the present context, since it turns into a comparison of stars lying at different distances, as shown in Pap-III. Hence, in the following we will always deal with CMa and the Warp as South/North overdensities.

Momany et al. (2004) confirmed that in the region  $220^\circ \leq l \leq 260^\circ$  there is a strong South/North asymmetry in the density of M giants but they attribute this overdensity to the maximum of the Galactic Warp. If this would be the case the extent of the global asymmetry should decrease for  $l > 260^\circ$ . The basic rationale of the present analysis can be summarised as follows: if the overdensity that we interpreted as the relic of a disrupting galaxy (CMa) is the effect of the maximum of the Warp-induced asymmetry, the well-defined RC feature shown in Fig. 1 (a) should be identifiable also in other regions dominated by the Warp and (b) should be associated with the largest global South/North asymmetry in star counts. In what follows we will compare the South *minus* North RC star counts around CMa ( $l \sim 240^\circ$ ) and in a region located in the broad maximum of the Warp asymmetry ( $l \sim 280^\circ$ , see López-Corredoira et al. (2002) and Pap-II) to verify the above hypothesis.

Fig. 2 shows such a comparison for two  $20^\circ \times 25^\circ$  fields centred at  $l = 240^\circ$  (left panels) and  $l = 280^\circ$  (right panels). The differences in the Southern and Northern Luminosity Functions (LF) of RC stars are presented in the J, H and K magnitude. Let us focus first on the right-hand panels of Fig. 2, showing a region outside of the main body of CMa and near the maximum of the Warp as identified by López-Corredoira et al. (2002). The excess of RC stars in the Southern hemisphere is already significant at  $K \simeq 11.0$  but it begins to grow strongly for  $K > 12.0$ , reaching 12000 stars per 0.2 mag bin at  $K = 15$ . The subtracted LFs (SLF) reveal the presence of a strong South/North asymmetry, with

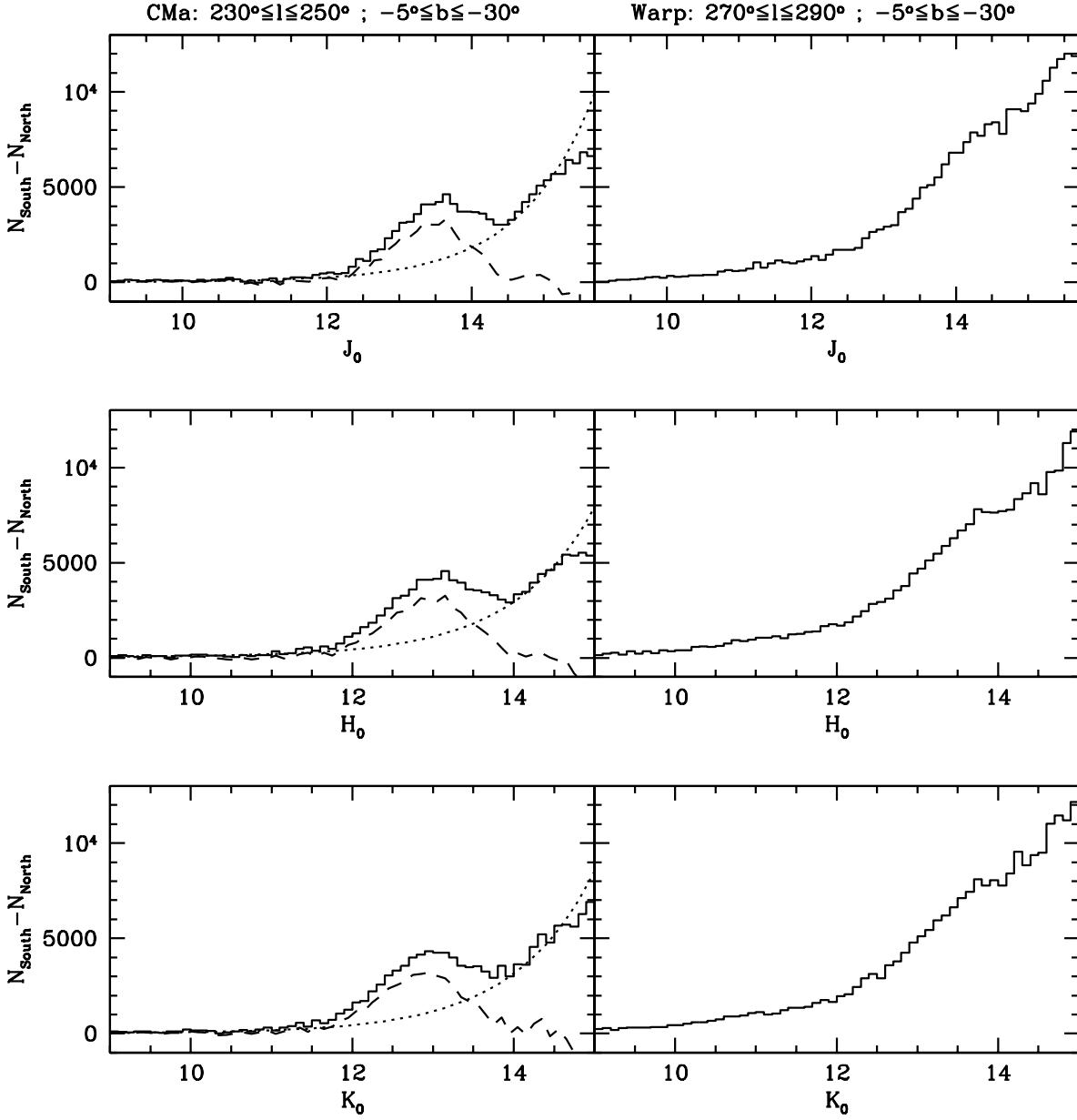


**Figure 2.** Subtracted Luminosity Functions (SLF histograms) of RC stars in J (upper panels), H (middle panels) and K (lower panels) for a field centred on the CMa structure (left panels) and around the region of maximum density of the Galactic Warp (right panels). Dotted lines are best-fit curves to the SLFs outside the range of magnitudes dominated by the CMa RC bump ( $11.5 \lesssim K \lesssim 14.0$ ); dashed lines are the residuals of the subtraction of the fitted curves to the observed SLFs. SLFs are the result of the subtraction of the LF of colour selected RC stars in a given field in the Southern Galactic hemisphere and the LF of the symmetric field in the Northern Galactic hemisphere (with respect to the Galactic Plane).

a characteristic behaviour as a function of magnitude that can be fit by exponential functions of the form

$$\Delta N_{S-N} = ae^K + bK + c. \quad (1)$$

This is the general form of the global South/North asymmetry, as traced by RC SLFs, in the range of Galactic latitudes considered here ( $220^\circ \leq l \leq 320^\circ$ ), as will be shown in Sect. 3, below.

The overall form of the subtracted LFs is the same in the  $l = 240^\circ$  field (left panels), but the amplitude of the

asymmetry is much lower here, reaching 7000 stars per bin at  $K = 15$ . On the other hand, a strong and significant broad bump is clearly observed, superposed on the exponential SLFs and centred around  $J \sim 13.5$ ,  $H \sim 13.0$ , and  $K \sim 12.7$  (see Pap-II). This bump has no counterpart in the  $l = 280^\circ$  field and is identified as the Red Clump of a spatially confined population, the Canis Major galaxy<sup>1</sup>. Note

<sup>1</sup> In Sect. 4 we will show that a *minor* component of the CMa RC population is in fact present also around  $l \sim 280^\circ$ . This is

that the comparison displayed in Fig. 2 is "doubly differential", i.e. it compares the South-North differences in RC star counts at different Galactic longitudes. We fit the underlying SLF outside the bump with Eqn. 1 (dotted lines) and subtract it from the observed SLF. The result is presented as a dashed line and shows essentially no residual outside the RC bump, while the bump itself contains (approximately) the same number of stars in the J, H and K SLFs. Hence, each band provide a quantitatively consistent view of the RC of CMa.

There are several features emerging from Fig. 2 that deserve more comment and interpretation:

- The overall South/North asymmetry in RC star counts is much stronger around  $l = 280^\circ$  than around CMa ( $l = 240^\circ$ ). Hence CMa cannot be identified as the maximum of the Galactic Warp seen as a South/North overdensity.
- The RC of CMa is clearly observed as an additional component superposed on the SLF characteristic of the underlying population (hereafter UP) that traces a South/North asymmetry that is visible on much larger scales and that we interpret as due to the Galactic Warp. This is the natural way we would perceive any stellar system that is placed in a region of the sky were the Warp asymmetry is present and strong as at  $l = 240^\circ$  (see López-Corredoira et al. 2002, and Sect. 4., below).
- By fitting the SLF of the underlying population outside the RC bump with Eqn. 1 and subtracting it from the overall SLF, we can attempt to disentangle the contribution of CMa and of the Warp to the total South/North asymmetry observed in this region of the Galaxy. This may help to obtain a better global view of both structures (see Sect. 3 and 4, below).
- The SLF in J, H, and K provide a fully self-consistent view of the asymmetries we are dealing with. For this reason, in the following we will limit our analysis to SLFs in K, the band that should be less affected by interstellar extinction.

### 3 PHYSICAL PARAMETERS OF CMA FROM THE RC STARS

#### 3.1 Distance

RC stars are widely used as distance indicators (see, for example Paczynski & Stanek 1998; Sarajedini et al. 2002; Babusiaux & Gilmore 2005, and references therein). In Pap-II we assumed  $M_K = -1.5 \pm 0.2$  for the RC of CMa, since, according to the theoretical models by Salaris & Girardi (2002), this interval encloses the absolute K magnitude of the RC for populations of metallicity  $-0.4 \lesssim [M/H] \lesssim -0.7$  and age between 4 Gyr and 10 Gyr, i.e. the proper age and metallicity for CMa (see Pap-II). Here we adopt the same assumption to convert the SLFs of Fig. 2 into the distance distributions displayed in Fig. 3. These distance distributions should be regarded with some caution since the adopted distance scale is optimised for the RC of CMa and may provide misleading answers when is applied (a) to contaminant sources that are not RC stars (see sect. 2, above), and (b)

not relevant in the present context where we outline the basis of the method that will allow us to disentangle the CMa population from the contamination due to Galactic stars.

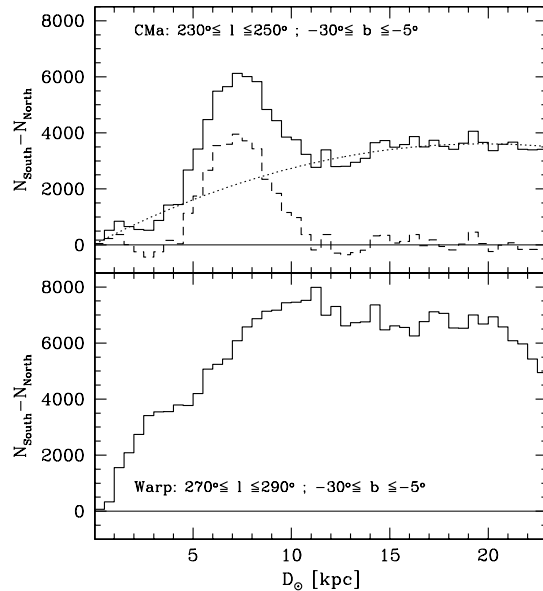


**Figure 3.** Distance distributions of South-North excess of RC stars in the same fields as Fig. 2. The dotted line is a fit to the distribution outside the CMa RC bump ( $5.0 \text{ kpc} \lesssim D_\odot \lesssim 11.0 \text{ kpc}$ ). The dashed line is the result of the subtraction of the fitted curve to the observed distance distribution, i.e. the profile of CMa along the line of sight.

to RC stars outside the age and metallicity ranges outlined above. For these reasons the backbone of the analysis carried on in the following sections is tied to the more reliable SLFs and not to distance distributions. On the other hand the latter should provide a general idea of the overall spatial distribution of RC stars in this region of the Galaxy and a reliable distance profile for the CMa system (see also Sect. 4.4, below).

The comparison of the two panels of Fig. 3 (upper panel: CMa+Warp; lower panel: "pure Warp") clearly confirms the main results of Fig. 2, i.e. the overall asymmetry is much stronger around  $l = 280^\circ$  than around  $l = 240^\circ$ , and the RC bump is clearly detected in the  $l = 240^\circ$  field while it is lacking in the  $l = 280^\circ$  field. The maximum amplitude of the UP asymmetry is reached at  $D_\odot \simeq 10 \text{ kpc}$  (corresponding to a galactocentric distance  $R_{GC} \simeq 11.6 \text{ kpc}$ ) and remains nearly constant at larger distances. We fit the distance distribution of the UP in the  $l = 240^\circ$  field with a second degree polynomial (dotted line). The subtraction of the fitted curve to the the observed distance distribution leaves a residual that is virtually null for  $D_\odot < 5.0 \text{ kpc}$  and  $D_\odot > 10.0 \text{ kpc}$ . Within these limits the bell-shaped distribution of CMa RC stars stand out very clearly, with a peak at  $D_\odot \simeq 7.2 \text{ kpc}$  (see Pap-III). The Half Width at Half Maximum of the distance distribution of CMa RC stars along the line of sight is  $\simeq 2 \text{ kpc}$ , in good agreement with the results of Pap-I.

There are two fundamental features emerging from Fig. 3 that should be noted:

- The distance profile of CMa as obtained from its RC stars is strikingly similar to that derived from M-giants in Pap-III. Even leaving aside the perfect coincidence of the

peaks of the two distributions, that may be ascribed to a mere coincidence within the uncertainties associated with the two distance scales, it remains a fact that the two independent tracers give essentially *the same* line-of-sight profile of the CMa system.

- In our various analyses we have obtained distance estimates for CMa from four different and independent distance indicators. In order of accuracy: from the tip of the Red Giant Branch in the I band ( $D_{\odot} \simeq 7.2$  kpc, Pap-III), from the Red Clump in K band ( $D_{\odot} \simeq 7.2$  kpc, present analysis), from the photometric parallax of M giants in the K band ( $D_{\odot} \simeq 7.1$  kpc, Pap-I), and from Main Sequence fitting in the B and V bands ( $D_{\odot} \simeq 7.6 - 8.7$ , Pap-II). All of these independent methods consistently provide a distance of the centre of CMa within 7.0 kpc and 9.0 kpc. Hence, the average distance of CMa should be now regarded as a very reliable piece of information about this system. Note that if  $D_{\odot} \simeq 7.2$  kpc is assumed, the age estimate obtained in Pap-II would shift toward older ages (i.e.  $6 \text{ Gyr} \lesssim \text{age} \lesssim 10 \text{ Gyr}$ , instead of  $4 \text{ Gyr} \lesssim \text{age} \lesssim 10 \text{ Gyr}$ ).

### 3.2 Luminosity and surface brightness

The Evolutionary Flux relation (Renzini & Buzzoni 1986; Renzini & Fusi Pecci 1988; Renzini 1998) states that the total number of stars in a given evolutionary phase  $j$  ( $N_j$ ) is proportional to the total luminosity of a stellar system ( $L_T$ ). Considering a Simple Stellar Population (SSP, i.e. a population of stars with the same age and chemical composition):

$$L_T = B(t)N_j t_j \quad (2)$$

where  $t_j$  is the duration of the evolutionary phase in years, and  $B(t)$  is the specific evolutionary flux, i.e. the number of stars entering or leaving any post Main Sequence evolutionary phase per year per solar luminosity as a function of time ( $t$ , i.e. the age of the SSP).

We can use Eqn. 2 to obtain a distance-independent estimate of the total luminosity of CMa from the RC star counts. With some algebra we obtain:

$$M_V = -2.5 \left[ \log[N_j] - \log\left[\frac{L_T}{L_V}\right] - \log[t_j] - \log[B(t)] \right] + M_{V\odot} \quad (3)$$

where  $M_V$  is the absolute integrated magnitude in the V-band and  $M_{V\odot}$  is the absolute V magnitude of the Sun. For the present case we adopt  $B(t) = 1.71 \times 10^{-11}$  and  $\frac{L_T}{L_V} = 1.5$  from the SSP models by Maraston (1998, 2005) with  $[M/H] = -0.33$ , age = 6.0 Gyr and Salpeter Initial Mass Function<sup>2</sup>.  $M_{V\odot} = 4.83$  is also adopted according to Maraston (1998), while the duration of the core He-burning phase ( $t_{HB} = 0.87 \times 10^8$  yrs) for a population with age  $\simeq 6.0$  Gyr and  $[M/H] = -0.35$  has been taken from Pietrinferni et al. (2004)<sup>3</sup>.

In the same way we can use Eqn. 5 by Renzini (1998) to obtain a distance-dependent estimate of the surface brightness near the centre of CMa ( $\mu_{V,0}$ ):

$$\mu_{V,0} = -2.5 \log(n_j) + 2.5 \log(\text{FoV}) + (m - M)_0 + \text{Norm} \quad (4)$$

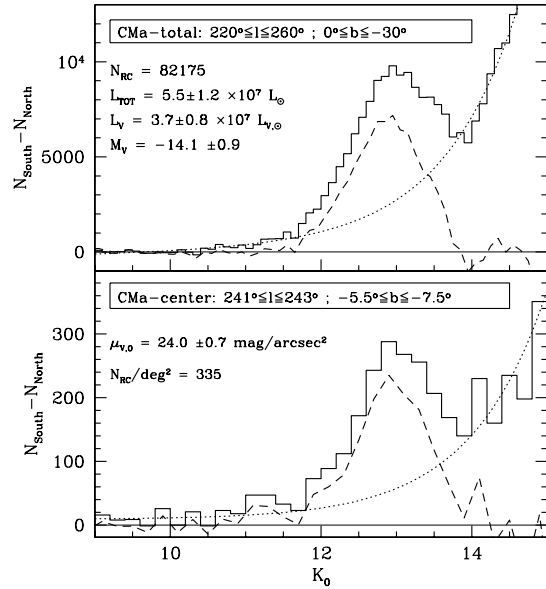


**Figure 4.** Subtracted Luminosity Functions of a field enclosing the whole main body of CMa (upper panel) and of a  $2^\circ \times 2^\circ$  field at the centre of CMa (lower panel). The symbols are the same as in Figs. 2 and 3.

where  $n_j$  is the number of stars in the  $j$  evolutionary phase within the considered Field of View (FoV, in  $\text{arcsec}^2$ , for example), and the term *Norm* encompasses all the theoretical assumptions:

$$\text{Norm} = 2.5 \log\left[\frac{L_T}{L_V}\right] + 2.5 \log[t_j] + 2.5 \log[B(t)] + M_{V\odot}$$

We assume the distance modulus  $(m - M)_0 = 14.3$ , as derived in Pap-III and in the present contribution.

The method adopted to estimate the observables required by Eqn. 3 and Eqn. 4 ( $N_{HB}$  and  $n_{HB}$ ) is displayed in Fig. 4. In the upper panel of Fig. 4 we fit Eqn. 1 to the SLF of the UP in the region  $220^\circ \leq l \leq 260^\circ$  and  $-30^\circ \leq b \leq 0^\circ$ . The residual RC population amounts to  $82175 \pm 287$  stars (Poisson noise), corresponding to a total luminosity of  $5.5 \pm 1.2 \times 10^7 L_{\odot}$  and to  $M_V = -14.1 \pm 0.9$ . This estimate is in excellent agreement with those obtained in Pap-I from M giants and by Martinez-Delgado et al. (2005) from optical photometry ( $M_V = -13.8 \pm 1.8$ ). In this case we have included in the computation also the  $|b| < 5^\circ$  region, for completeness. The inclusion or exclusion of this region in the estimate changes the value of the V-band integrated magnitude by  $\sim \pm 0.5$  mag. The above estimate of the total luminosity of CMa should be considered as a lower limit since (a) the main body of the galaxy may extend by a few degrees beyond  $l = 260^\circ$  (see Sect. 4.2, below), (b) it may partially extend also beyond  $b = 0^\circ$  into the Northern hemisphere where it is inaccessible to the SLF technique adopted here (Pap-I), and (c) there may be a (still undetected) minority of Horizontal Branch stars that are not in the Red Clump (RR Lyrae and/or Blue Horizontal Branch stars, see, for example Mateu et al. 2005). However the adopted window and source-selection certainly accounts for the bulk of the CMa system.

<sup>2</sup> see <http://www.mpe.mpg.de/~maraston/SSP>

<sup>3</sup> see <http://www.te.astro.it/BASTI/>

In the lower panel of Fig. 4 we apply the same technique as above to a  $2^\circ \times 2^\circ$  field located at the centre of CMa as identified in Pap-I ( $l = 242.0^\circ; b = -6.5^\circ$ )<sup>4</sup>. We find a surface number density of  $335 \pm 18$  RC stars per square degree, corresponding to a surface brightness of  $\mu_V = 24.0 \pm 0.7$  mag/arcsec<sup>2</sup>, again in good agreement with the independent results by Martínez-Delgado et al. (2005,  $\mu_{V,0} = 24.1 \pm 1.8$  mag/arcsec<sup>2</sup>).

Note that  $B(t)$ , at fixed  $[M/H] = -0.33$ , varies from  $1.66 \times 10^{-11}$  at  $t = 1.0$  Gyr to  $1.75 \times 10^{-11}$  at  $t = 13.0$  Gyr, and, for fixed age = 6.0 Gyr, it ranges from  $1.66 \times 10^{-11}$  at  $[M/H] = -1.35$  to  $1.98 \times 10^{-11}$  at  $[M/H] = +0.35$ . The variation of  $t_{HB}$  over the same range of age and metallicity is just of a few per cent (Pietrinferni et al. 2004). Hence the particular choices of the above parameters do not seriously affect our final estimates. In any case, the reported final uncertainties also take these factors into account.

CMa turns out to have a total luminosity and a surface brightness quite similar to those of the Sgr dSph, as already noted in Pap-I, but the above results suggest that it may be slightly more luminous and with a brighter  $\mu_{V,0}$ , in agreement with the  $M_V$  vs.  $\mu_{V,0}$  relation of dwarf spheroidal galaxies (see Martínez-Delgado et al. 2005, and references therein). It is interesting to note the striking effect of the relative distance on the number densities for two stellar systems of similar central surface brightness. Monaco et al. (2003) measured a density of RC stars of  $\simeq 2100$  deg<sup>-2</sup> in the central degree of the Sgr dSph, while here we observe just  $335$  deg<sup>-2</sup>, yet the surface brightness of the two systems is similar. This may largely account for the great difficulty in the identification of the RC in optical CMDs from off-centred fields of  $0.25$  deg<sup>2</sup> or less as those presented in Pap-II and in Martínez-Delgado et al. (2005). This argument will be developed in larger detail in Sect. 4.3, below.

In summary, the quantitative and qualitative picture of the Canis Major system that we have obtained using Red Clump stars is fully consistent with the results obtained using M giants in Pap-I and Pap-III and using MS stars in Pap-II and in Martínez-Delgado et al. (2005). It is fully confirmed that CMa is a stellar system having luminosity, surface brightness and size typical of a dwarf spheroidal galaxy, being located at  $\sim 7-8$  kpc from the Sun, in front of most of the "sloped screen" of the warped lobe of the Galactic disc we see in that direction. In the following Section we will study its relation with the large scale South/North asymmetry produced by the Galactic Warp, that we trace as the underlying population in our SLFs.

#### 4 CMA AND THE GALACTIC WARP

The technique adopted above to disentangle the contribution of the Warp and of CMa to the overdensity of RC stars observed in the considered region of the Galaxy should be used with great caution. While the applications presented

in the previous sections are straightforward, a more general use is less secure. In particular, a reliable disentanglement of the signals from the two populations contributing to the SLFs can be performed only in regions where (a) the signal associated with the UP is strong and clearly characterised and, (b) the signal from the CMa RC peak is at least as strong as that coming from the UP in the same magnitude range. Lacking one or both of the above conditions may lead to very uncertain or misleading results. For instance, in a region where the signal from CMa is weak, a feature of the SLF of the UP can be misinterpreted as due to CMa. It has to be recalled that there is no physical meaning attached to Eqn. 1 that we use to model the SLF of the UP, it is just a convenient parametrisation. The actual form of the SLF depends on the structure of the Galaxy and on the stellar populations encountered along a given line of sight, so one must be careful not to over-interpret the results presented below. Our intent is to provide a general and global description of the behaviour of the two overdensities we are currently dealing with, CMa and the Warp, as traced by RC stars and we are conscious of the limits of the adopted technique. In particular, we are interested in the relative surface density of the two structures at different longitudes and to their approximate characteristic scales.

With these caveats in mind, we present in Fig. 5 the SLFs of  $10^\circ \times 10^\circ$  fields sampling the whole range of Galactic longitudes considered by the present study in the latitude window  $-15^\circ \leq b \leq -5^\circ$ . The fit of the UP SLFs is presented as a dotted line and the residual of the subtraction of the fitted curve to the observed SLFs as a dashed line, as in the plots presented in previous sections. The RC peak of CMa is clearly the dominant contributor to the observed South/North asymmetry in the range  $11.5 \leq K \leq 14.0$  between  $l = 220^\circ$  and  $l = 270^\circ$ . For  $l > 270^\circ$  any signal from the CMa RC peak is overwhelmed by the contribution of the UP, and for  $l \geq 280^\circ$  it has essentially disappeared. The UP overdensity steadily grows from  $l \sim 230^\circ$  to  $l \sim 290^\circ$  and then fades at larger longitudes, but at  $l \sim 315^\circ$  is still strong and significant. The only exception to this general trend is the slightly higher signal of the UP in the  $l = 225^\circ$  field with respect to the  $l = 235^\circ$  field around  $K \sim 14.0$  that may be due to some substructure in the Warp (or in the Ring, see Fig. 7, Fig. 11 and Fig. 12, below) along that line of sight.

It is clear that the LFs of the UP trace an overdensity with a global scale larger than the range of Galactic longitudes considered here ( $220^\circ \leq l \leq 320^\circ$ ), it is detected in the whole sampled range of magnitudes and reaches its maximum around  $l \sim 290^\circ$ . The absence of any feature in the SLF for  $l \geq 280^\circ$  and the global nature of the overdensity traced by the UP points toward its identification with a structure of the Galactic disc, namely the stellar Warp as described by López-Corredoira et al. (2002). The detection of a maximum at  $l \sim 290^\circ$  is in good agreement with that found by López-Corredoira et al. (2002) and Vig, Ghosh & Ojha (2005). On the other hand the CMa population is associated with a well-defined feature (bump) in the SLF that is confined to a much smaller range of longitudes. To obtain a more quantitative and readily-interpretable view of the above results we separate (using the fit to the UP SLF) the contribution of the UP and of the CMa RC in the range enclosing the RC peak ( $11.5 \leq K \leq 14.0$ ). The number of CMa RC stars (the residuals of the SLF fits of Fig. 5)

<sup>4</sup> The exact centre of the system cannot be identified very accurately with the extant data, see Pap-I and Sect. 4.2, below. However we find essentially the same surface brightness for fields within  $240^\circ \leq l \leq 250^\circ$  and  $-8.5^\circ \leq b \leq -5.5^\circ$ . Here we chose a field at  $l = 242^\circ$  and  $b = -6.5^\circ$  because of the low extinction in this region (see Figs. 8 and 9, below).

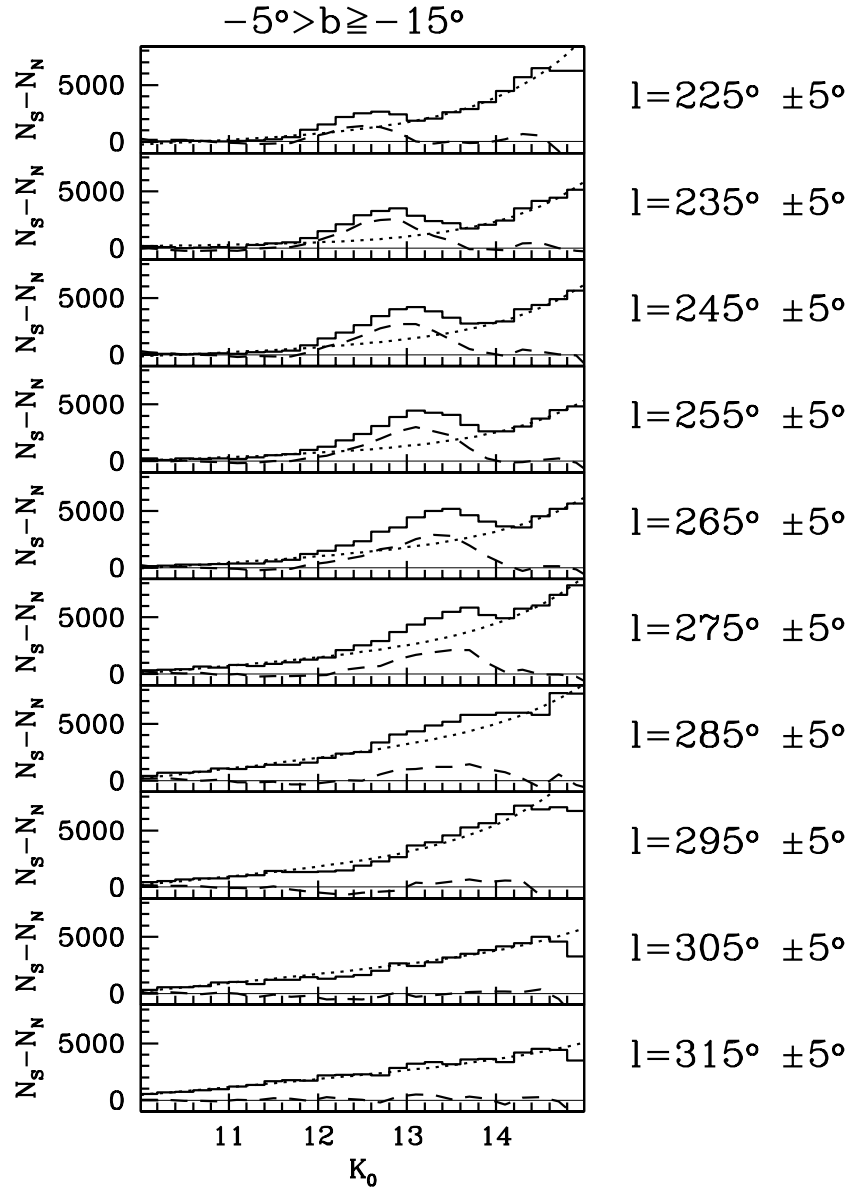


**Figure 5.** SLFs as a function of Galactic longitude. The symbols are the same as in Figs. 2, 3 and 4.

per field in the above magnitude range, and the number of UP stars in the same range (computed from the fit itself) are plotted as a function of Galactic longitude in Fig. 6 (as filled triangles and open circles, respectively). The feature that emerges more clearly here compared to the analysis of Fig. 5, is that the UP reaches much larger surface density values than CMa (for  $l > 270^\circ$ ) and even around the core of CMa the surface density of the two contributors is of the same order. This indicates that the UP traces a much stronger and extended asymmetry with respect to CMa, as expected from a Galactic-scale feature integrated over a wide range of distances (note that, according to Fig. 3, most of the overdensity associated with the UP lies *behind* CMa, at  $D_\odot \gtrsim 10$  kpc). Hence, the global view of the South/North asymmetries provided by Figs. 5 and 6 confirms that the

CMa overdensity is of different nature with respect to the large-scale overdensity associated with the UP. This is fully consistent and confirms the conclusions drawn in Pap-II, Pap-III and in Sect. 3, above, i.e. the CMa overdensity is due to the relic of a dwarf galaxy seen on top of the larger and more extended asymmetry due to the Galactic Warp. In Sect. 4.2 we will apply the same technique used to obtain the surface densities of RC stars plotted in Fig. 6 to map the two dimensional structure of CMa and the Warp, disentangling the contributions of CMa and of the UP in the same magnitude range by fitting Eqn. 1 to the SLF of the UP.

The success of the adopted technique suggests that the CMa population (its putative tidal stream, in particular) can perhaps be traced with RC stars also at lower Galactic



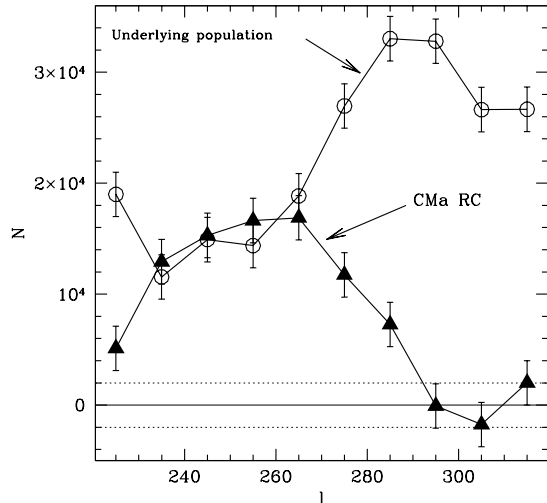


**Figure 6.** Star counts from the SLFs of Fig. 5 within  $11.5 \leq K \leq 14.0$  as a function of Galactic longitude. Filled circles: CMa Red Clump, Open circles: Underlying Population. The dotted lines enclose the typical range of uncertainties due to the subtraction of the fitted curves (Eqn. 1, dotted curves in Fig. 5) to the observed SLFs.

longitudes ( $l < 220^\circ$ ). However, we focus the present contribution on the core of CMa and on its relation with the Warp, deferring the study of the fields toward the Galactic Anticentre to a future investigation.

#### 4.1 The spatial orientation of CMa

There are two further features in the SLFs of Fig. 5 that deserve a comment.

First, the peak of the RC bump shifts to larger magnitudes (distances) at larger longitudes, from  $D_\odot \sim 6.5$  kpc at  $l \sim 225^\circ$  to  $D_\odot \sim 9.5$  kpc at  $l \sim 265^\circ$ . This may reflect the spatial orientation of the major axis of CMa with respect to the line of sight. To check this point we fitted Gaussian curves to the residuals of the subtraction of the UP model to the observed SLF of Fig. 5 in the range of longitudes where the signal from CMa RC is larger than that provided by the UP ( $220^\circ \leq l \leq 270^\circ$ , i.e. in the main body of CMa). We converted the K magnitudes of the peak of the fitted Gaussians into distance moduli and distances with the same assumptions adopted in Sect. 3.1 (see Table 1 for the results). While the observed residuals significantly depart in some cases from a Gaussian shape, the position of the peak is reliably derived, with typical uncertainties of  $\pm 0.05$  mag. On the other hand, the estimated  $\sigma$  should be considered just as an indication of the width of the distributions.

In the upper panel of Fig. 7 the *distance-longitude* gradient observed in the main body of CMa (filled circles) is compared with the results of the N-body simulation of the disruption of the CMa galaxy presented in Pap-IV. The simulation is produced by a dwarf galaxy model of mass  $5 \times 10^8 M_\odot$  that is accreted onto the Milky Way during  $\sim 3$

**Table 1.** Distances of the CMa RC peaks detected in Figure 5.

$\langle l \rangle$	$K_{peak}^{Gauss}$	$\sigma_K$	$D_\odot$ [kpc]
$225^\circ$	12.50	0.35	$6.3 \pm 1.1$ <sup>a</sup>
$235^\circ$	12.75	0.44	$7.1 \pm 1.1$
$245^\circ$	12.97	0.46	$7.8 \pm 1.2$
$255^\circ$	13.10	0.48	$8.3 \pm 1.2$
$265^\circ$	13.35	0.50	$9.3 \pm 1.2$

<sup>a</sup> The uncertainties on the distances have been obtained adding the formal uncertainties from the fit of the position of the peak to an arbitrary 1 kpc error that should account for the uncertainties associated with the distance scale and with the SLF fit+subtraction process.

Gyr (see Pap-IV for details) and it was built to reproduce the current mean position and 3-D velocity of CMa as well as the *distance-radial velocity* gradient discovered in Pap-IV. Hence the *distance-longitude* behaviour of the remnant is a *prediction* of the model, not an *a priori* requirement. Therefore the excellent qualitative and quantitative agreement with the *observed* and *predicted* spatial orientation of the main body of CMa may be considered as a success of the dwarf-galaxy-accretion scenario for the nature of CMa. In other words, the shift of the RC peak with Galactic longitude observed in Fig. 5 is fully consistent with the model of a disrupting dwarf galaxy that fits the observed position and kinematics of CMa.

Second, the RC bump broadens with increasing longitude. Since, as we have shown above, the average distance of CMa also increases with increasing longitude, one would expect the opposite effect if the considered lines of sight sampled a distribution of stars with constant physical width, due to the compression effect of the magnitude scale. However the observed broadening is a much less reliable indicator with respect to the position of the peak, since several spurious factors may contribute to it. While shifting to fainter magnitude and higher longitudes, (a) the increasing photometric errors, (b) the increasing contribution of the UP in the magnitude range of the bump, and (c) the increasing number of unrelated sources that may contaminate our colour-selected RC sample, should all contribute to the smearing of the RC peak. In any case, the lower panel of Fig. 7 suggests that part of the effect may be also due to the orientation of the remnant with respect to the different lines of sight (l.o.s.). According to the model of Pap-IV, the angle between the l.o.s. and the major axis of the remnant ranges from nearly  $90^\circ$  at  $l = 220^\circ$  to  $\sim 30^\circ$  at  $l = 280^\circ$  and the width of the distance distribution along the l.o.s. should consequently increase for this reason.

Finally, the simulation of Pap-IV (as that of Pap-I and of Penarrubia et al. 2005) predicts that the tidal tails of the disrupting dwarf galaxy are multiply wrapped around the Milky Way, so that different structures may be observed at different distances along the line of sight. These effects may be at the origin of the anomaly detected in the SLF at  $l = 225^\circ$  around  $K \sim 14.0$  (see Fig. 5, compare with the simulation around  $l = 225^\circ$  in the upper panel of Fig. 7).

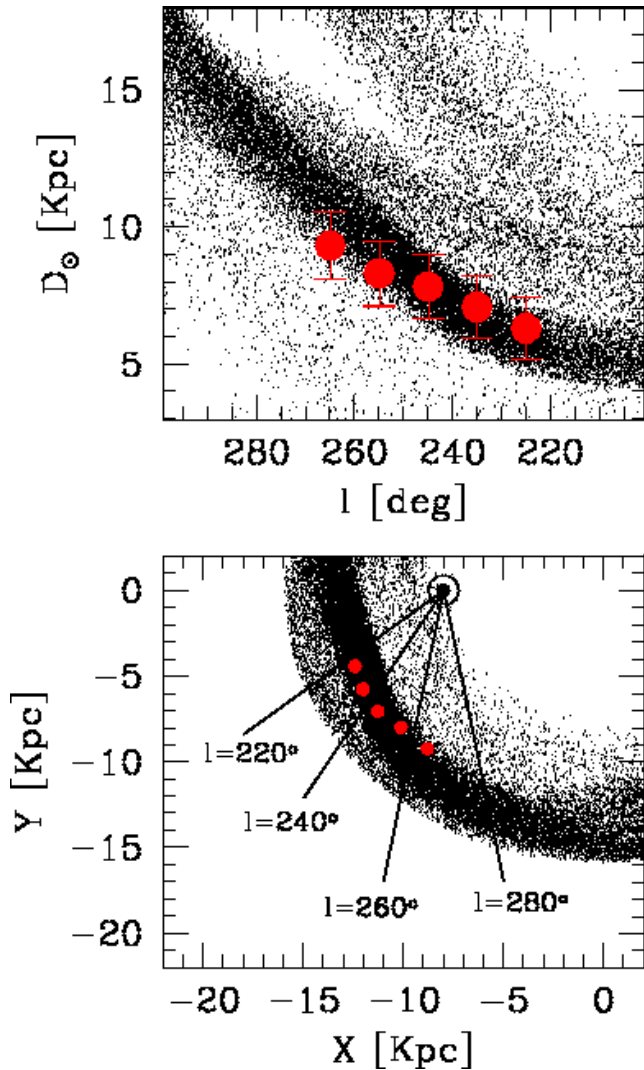


**Figure 7.** The spatial orientation of the main body of CMA as traced by RC stars (filled circles) is compared with the N-body model of the disruption of the CMA dwarf galaxy presented in Pap-IV (small dots). Upper panel: Heliocentric distance as a function of Galactic longitude. Lower panel: X,Y projection; in this reference system the Galactic Centre is located at (0,0,0) and the Sun at (-8.0;0,0). For the sake of clarity, only model particles with Galactocentric distance  $R_{GC} \leq 16.0$  kpc are plotted. The directions of the lines of sight toward  $l = 220^\circ, 240^\circ, 260^\circ$  and  $280^\circ$  are plotted to show the effect of the orientation on the line-of-sight profile of CMA.

#### 4.2 Two-dimensional structure

To obtain a two-dimensional map of CMA and the Warp we push the “fit and subtract” technique we applied to the SLFs in previous sections to the extreme application allowed by the data. We divided the region within  $220^\circ \leq l \leq 320^\circ$  and  $-20^\circ \leq b \leq 0^\circ$  into a grid of  $49 \times 9$  boxes of dimension  $4^\circ \times 4^\circ$ , spaced by  $2^\circ$  steps both in  $l$  and  $b$ . For each box we derived the SLF and we fitted it, outside the RC bump region, with Eqn. 1. Then, by subtracting the fitted curve to the observed SLF we obtained the number of stars in the box associated with the CMA RC and with the UP (Warp) within the range  $11.5 \leq K \leq 14.0$ , as done in Figs. 5 and

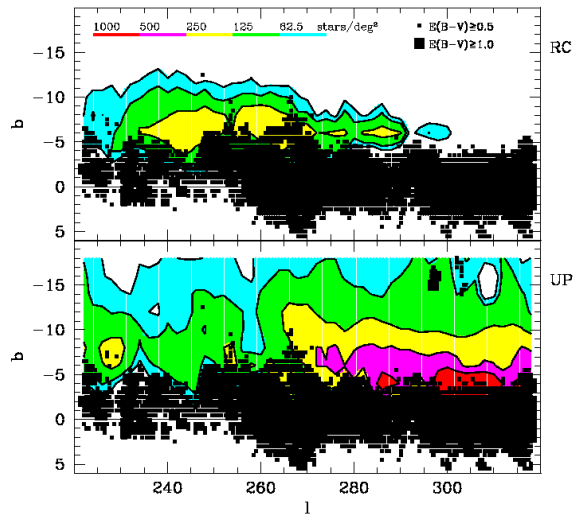


**Figure 8.** Density maps of RC stars in the range  $11.5 \leq K \leq 14.0$ , in terms of star counts per square degree. Small squares mark positions where the reddening is  $0.5 \leq E(B-V) < 1.0$ , large squares correspond to reddenings in excess of 1.0 mag. Upper panel: map of the CMA RC population; Lower panel: map of the Underlying Population (Warp).

6, above. The uncertainties in the surface number densities ( $\sigma$ ) were obtained by propagating the Poisson noise of the star counts and taking into account the uncertainty of the fit+subtraction process.

It should be noted that the caveats described at the beginning of Sect. 4 are even more valid in this case where SLFs are obtained from much smaller fields compared to Fig. 5. Moreover, we included in this analysis, for completeness, also the  $|b| < 5^\circ$  fields which are affected by large amounts of extinction. On the other hand, *each* of the 441 SLFs from which we derived our maps was carefully inspected and we are confident that the final surface densities reliably describe the broad two-dimensional structure of the two considered overdensities, at least for boxes centred at  $b \leq -6^\circ$ . In the two rows of boxes closer to the Galactic Plane (i.e., those centered at  $b = -2^\circ$  and, to a lesser extent,  $b = -4^\circ$ ) the high degree of crowding seems to affect seriously the completeness properties of the samples. The densities derived there are more uncertain but have little effect on the conclusions we draw in this Section. In a few cases (6-8 boxes over 441, with  $b \leq -16^\circ$ ) the low statistics prevented a satisfactory disentanglement of the two considered components: we lowered the statistical weight of these points of the grid by artificially enhancing the associated  $\sigma$ .

We present our maps into two different forms, depending on the aim of the analysis. To compare the relative densities and extensions of CMA and the Warp we produce a total map in terms of  $\text{stars}/\text{deg}^{-2}$  (Fig. 8). To obtain the most reliable view of the structure of CMA we use a map with an enlarged scale in units of  $\sigma$  (Fig. 9). In this way we can consider just the overdensities with the largest statistical significance. This seems particularly advisable given

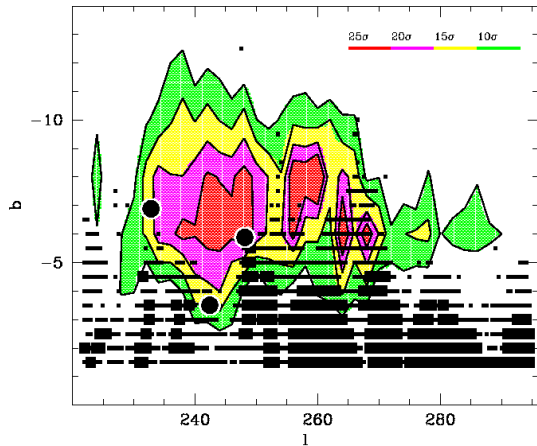


**Figure 9.** Density map of CMA RC stars in terms of statistical significance ( $\sigma$  units). Small squares mark positions where the reddening is  $0.5 \leq E(B - V) < 1.0$ , large squares correspond to reddenings in excess of 1.0 mag. Large filled circles mark the position of three old open clusters that project onto the main body of CMA and have distances within the CMA profile shown in Fig. 3; in order of increasing longitude (i.e. from left to right): Tombaugh 2, Haffner 11 and Arp-Madore 2.

the complex process that led to the estimate of the surface density of RC stars for the two considered components. To give a direct idea of the possible impact of the extinction on the detection of the structures in our fields we plot in both maps the distribution of reddening for  $E(B - V) \geq 0.5$ . Note that  $E(B - V) \leq 0.5$  corresponds to  $A_K \leq 0.17$  mag, hence the affect of extinction on the SLFs in regions with  $E(B - V) \leq 0.5$  should be negligible.

The maps presented in Fig. 8 nicely confirm the results shown in Figs. 5 and 6. The Warp is a much stronger and more extended overdensity with respect to CMA, with a maximum density around  $l \sim 290^\circ - 310^\circ$ . It is interesting to note that the Warp reaches its maximum surface density at lower  $|b|$  with respect to CMA, in agreement with the results of López-Corredoira et al. (2002) who found that the Warp South/North asymmetry is stronger at  $b = -3^\circ$  than at  $b = -9^\circ$ , toward  $l \sim 290^\circ$ . On the other hand, CMA reaches its maximum density in the range  $-5^\circ \leq b \leq -8^\circ$  (see Fig. 9, below). The Warp is seen to extend over the whole considered region of sky with surface density comparable (or larger) than CMA. The maps confirm that CMA is a smaller-scale overdensity on top of the Galactic Warp.

For a closer view of the CMA galaxy we turn our attention to Fig. 9. The densest regions of the map correspond to  $25\sigma$  overdensities, similar to what was found in Pap-I. The main body of CMA is separated into two large structures (centred around  $l \sim 245^\circ$  and  $l \sim 257^\circ$ , respectively) by a small region of high extinction located at  $(l, b) \sim (250^\circ, -3^\circ)$ , with a finger extending up to  $b \simeq -10^\circ$ . It is very likely that this separation is an artefact due to

these structures in the distribution of the interstellar dust. The bulk of the main body of the galaxy is enclosed within  $230^\circ \leq l \leq 260^\circ$ , in excellent agreement with the results of Pap-I. We also note that Fig. 9 fully supports our tentative detection of the CMA population (and in particular of the Red Clump of CMA) in the background of the open cluster NGC 2477, presented and discussed in Pap-II. The narrow structures detected around  $b = -5^\circ$ , from  $l > 260^\circ$  out to  $l < 290^\circ$  may be part of the associated tidal stream and are probably the counterparts of those seen in Fig. 5 of Pap-I at the same position. Any (minor) difference with the results of Pap-I may be due (a) to the different technique and tracer adopted, (b) to the exclusion of regions with  $E(B - V) > 0.555$  from the analysis of Pap-I, and (c) to the higher overall reddening assumed in Pap-I, where the correction by Bonifacio, Monai & Beers (2000) was not adopted. In any case there is no substantial difference between the view of CMA obtained with M giants and with RC stars.

We derived the barycentre of the surface brightness distribution of CMA in the range  $220^\circ \leq l \leq 270^\circ$  by averaging over the  $N = 216$  boxes in this region of the map:

$$\langle l \rangle = \frac{\sum_{i=1}^N l_i n_i}{\sum_{i=1}^N n_i} = 248.1^\circ \pm 2.0^\circ \quad (5)$$

$$\langle b \rangle = \frac{\sum_{i=1}^N b_i n_i}{\sum_{i=1}^N n_i} = -7.1^\circ \pm 0.3^\circ \quad (6)$$

where the uncertainties have been estimated with a bootstrap technique<sup>5</sup>. This is the best estimate of the approximate position of the centre of the main body of CMA as traced by Red Clump stars. Given the caveats stated above, this estimate should be taken just as an educated guess.

#### 4.2.1 Old open clusters in CMA

The possible association of some old open clusters with CMA was already suggested in Pap-I (see also Pap-II; Crane et al. 2003; Frinchaboy et al. 2004). A thorough analysis of these clusters is clearly beyond the scope of the present contribution. However, the use of the Red Clump as a tracer may provide the unique opportunity of placing a few clusters onto the same distance scale as the field population of CMA. In Table 2 we list a number of open clusters selected to be older than  $\sim 0.8$  Gyr and to lie in the surroundings of the main body of CMA (according to the WEBDA database, Mermilliod 1995). In particular the first group presented in Tab. 2 is composed of three clusters that directly project onto the main body of CMA (represented as large filled circles in Fig. 9), and for which it has been possible to estimate the K magnitude of the Red Clump from 2MASS photometry. Hence the distance estimates for To 2, AM 2 and Haf 11 have been derived in exactly the same way and under the same assumptions (luminosity of the standard candle and reddening) used for the analysis of the field population performed above. These estimates strongly indicate that To 2, AM 2 and Haf 11 are physically located within the main

<sup>5</sup> The quoted uncertainties are the standard deviations of the results of the application of Eqns. 5 and 6 to 1000 sub-samples of 100 boxes, randomly extracted from the 216 boxes of the considered portion of the map.

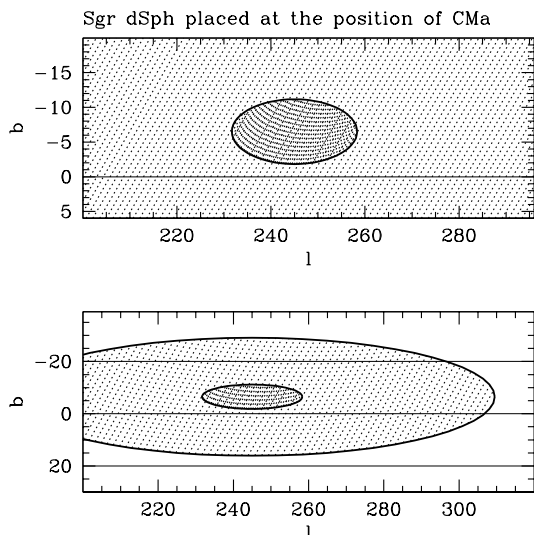


**Figure 10.** The appearance of the Sgr dSph if it were placed at the distance and position of CMa. The inner ellipse encloses the core of the galaxy (densely-shaded region), the outer ellipse is the limiting contour (sparsely shaded region; Sgr parameters from Majewski et al. 2003). The upper panel has the same longitude scale as Fig. 9 while the lower panel has the same longitude scale as Fig. 8, to allow a direct comparison with the maps shown there.

body of CMa (see Pap-II for further discussion and references). Note that, while AM 2 and Haf 11 lack any radial velocity estimate, To 2 has  $V_r \simeq +114$  km/s, fully consistent with the systemic velocity of CMa.

### 4.3 How should a nearby galaxy appear?

CMa is by far the nearest dwarf galaxy known, a factor  $\simeq 3.6$  closer than the previous “record holder”, the Sgr dSph (Monaco et al. 2004). This is the main reason why it appears so unusual, at first glance: a structure covering tens of degrees on the sky and with as few as  $\sim 300$  RC stars in its central square degree. This is very far from our idea of the typical dwarf satellite of the Milky Way, that has been acquired by studying much more distant examples. To show that there is nothing unusual in CMa except its distance we undertook the exercise of seeing how the Sgr dSph galaxy would appear if it were placed at the same distance and position as CMa. In the following we will adopt the structural parameters of Sgr (core radius  $r_c$ , limiting radius  $r_t$ , central surface brightness and axis ratio) as derived by Majewski et al. (2003), the distance from Monaco et al. (2004) and the surface density of Horizontal Branch stars from Monaco et al. (2003).

Fig. 10 shows the core and the limiting contours of Sgr once placed at the distance and position of CMa. The upper panel of Fig. 10 has the same longitude scale as Fig. 9 and the lower panel has the same longitude scale as Fig. 8, to allow a direct comparison. The core of the “mock” Sgr shows a major axis of more than  $\sim 26^\circ$  ( $r_c = 13.3^\circ$ ) and the over-

all appearance is strikingly similar to CMa. Note that the limiting contour extends well beyond  $l = 300^\circ$  ( $r_t = 64.5^\circ$ ).

It is intriguing to note that the size of the CMa contours in the latitude direction (Fig. 9) seem to shrink going from  $l \sim 240^\circ$  to  $l \sim 260^\circ$  (by a factor  $\sim 1.3$ ). This is approximately the expected effect of the distance-longitude gradient discussed in Sect. 4.1, i.e. a given linear dimension would subtend a smaller angle if placed at a larger distance. The observed gradient implies a shrinking of a factor  $\sim 1.2$  between  $l \sim 240^\circ$  to  $l \sim 260^\circ$ , in agreement with the map of Fig. 9. This effect is not included in Fig. 10 where the mean distance  $D_\odot = 7.2$  kpc has been assumed for CMa as a whole.

From Eqn. 4 the following relation can be derived between the surface brightness (at any chosen wavelength  $\lambda$ )  $\mu_{\lambda,1}$ ,  $\mu_{\lambda,2}$  and the number of stars per given area in a given evolutionary phase ( $n_1, n_2$ ) for two stellar systems located at distances  $d_1$  and  $d_2$ :

$$\mu_{\lambda,1} - \mu_{\lambda,2} = -2.5 \log(n_1/n_2) + 5 \log(d_1/d_2) \quad (7)$$

The second term on the right hand side of Eqn. 7 displays the effect of distance on the number surface density of a system of a given surface brightness<sup>6</sup>. To rescale the number surface density of Sgr from  $d_2 = 26.3$  kpc to  $d_1 = 7.2$  kpc we must assume  $\mu_{\lambda,1} - \mu_{\lambda,2} = 0.0$ . In the present case we find that the observed surface number density of Sgr stars should be reduced by a factor 0.075, if the galaxy is placed at the distance of CMa. Hence, in this case, we would observe  $\sim 150$  RC stars  $deg^{-2}$ , 10 RR Lyrae  $deg^{-2}$  and 12 Blue Horizontal Branch stars  $deg^{-2}$  in the centre of the Sgr galaxy, that is the surface number density would be even lower than what is observed in CMa (due to the difference in  $\mu_{V,0}$  discussed in Sect. 3.2). This effect fully accounts for the difficulty of detecting clearly-defined sequences of evolved stars in small fields (smaller than  $1 deg^2$ ) even within the main body of CMa, as well as for the poor results of searches of rare stellar species (as RR Lyrae stars in a system dominated by an intermediate-age and metal rich population, see Kinman, Saha & Pier 2004; Mateu et al. 2005).

In conclusion, the apparent size of CMa and the number density of its stellar populations are fully compatible with those of a dwarf galaxy similar to Sgr and located at 7.2 kpc from us.

### 4.4 The 3-D structure of Canis Major

Even keeping in mind the caveats described in Sect. 3.1, it is clear that RC stars provide quite reliable distances, in particular they are much less sensitive to metallicity and age variations in the considered populations compared to M-giants (see, Majewski et al. 2003; Crane et al. 2003; Martin et al. 2004a; Rocha-Pinto et al. 2005, and references therein). Therefore, we can use the distances of individual RC stars in our sample to obtain their Cartesian Heliocentric coordinates: 5

<sup>6</sup> It has to be noted that the effect of the physical size of a system on the spread of sequences on a CMD weakens with increasing distance. This is an additional factor that favours the easier recognition of distant stellar structures compared to more nearby systems.

**Table 2.** Old open clusters around the main body of CMa.

Name	$l^\circ$	$b^\circ$	E(B-V)	$K_0^{RC}$	$(m - M)_0$	$D_{sun}$ [kpc]
Tombaugh 2	232.83	-6.88	0.29	$12.95 \pm 0.10$	$14.45 \pm 0.22$	$7.76 \pm 0.8$
Haffner 11	242.39	-3.54	0.57	$12.20 \pm 0.20$	$13.70 \pm 0.28$	$5.49 \pm 0.8$
Arp-Madore 2	248.12	-5.88	0.51	$13.65 \pm 0.10$	$15.15 \pm 0.22$	$10.71 \pm 1.1$
Berekeley 36	227.38	-0.59				6.1
NGC 2243	239.48	-18.01				4.4
Melotte 66	259.56	-14.24				4.3
Ruprecht 75	276.79	-4.48				4.3
CC06	238.48	-4.28				4.5
Van den Bergh-Hagen 66	276.00	-3.01				7.0
Saurer 2	257.99	-1.01				4.8

<sup>a</sup>

<sup>a</sup> All the reported data, with the exception of those relative to the RC distance of To 2, AM 2 and Haf 11, are drawn from the WEBDA database (Mermilliod 1995), see <http://obswww.unige.ch/webda/>. Data for CC06 are from (Ivanov et al. 2002). First group: clusters within  $230^\circ \leq l \leq 260^\circ$ ,  $-12^\circ \leq b \leq 3^\circ$  and  $4.0 \text{ kpc} \leq D_{sun} \leq 11.0 \text{ kpc}$ , with age  $\geq 1 \text{ Gyr}$ . Second group: clusters within  $220^\circ \leq l \leq 280^\circ$ ,  $-20^\circ \leq b \leq 0^\circ$  and  $4.0 \text{ kpc} \leq D_{sun} \leq 11.0 \text{ kpc}$ , with age  $\geq 0.8 \text{ Gyr}$ .

$$x = D_\odot \cos(l) \cos(b) [\text{kpc}] \quad (8)$$

$$y = D_\odot \sin(l) \cos(b) [\text{kpc}] \quad (9)$$

$$z = D_\odot \sin(b) [\text{kpc}] \quad (10)$$

In this system the coordinates of the Sun are  $(x,y,z)=(0,0,0,0,0)$  and the centre of the Galaxy is located at  $(x,y,z)=(+8,0,0,0,0)$ , having assumed that the distance to the Galactic center is 8 kpc. We selected, in both hemispheres, only the RC stars having  $5^\circ \leq |b| \leq 15^\circ$ , to avoid the regions of higher extinction and to include the densest parts of the overdensities we are dealing with (see Fig. 8). To avoid any possible effect of local inhomogeneities in the vicinity of the Galactic Plane we also removed the stars having  $|z| < 0.5 \text{ kpc}$ . Given the adopted selections this is equivalent to excluding stars within  $\simeq 1 \text{ kpc}$  from the Sun.

From these samples we computed the density of RC stars on an  $x,y$  grid with boxes of size  $1 \text{ kpc} \times 1 \text{ kpc}$ , spaced by  $0.5 \text{ kpc}$  both in  $x$  and in  $y$ . In this way we obtained  $x,y$  density maps of the Southern and Northern Hemisphere that can be subtracted, "pixel-to-pixel", to obtain a map of the residual surface density in the  $x,y$  plane. To focus our attention only on highly statistically significant residuals we produced a residual density map in units of  $\sigma$ , as in Fig. 9. The density at each point of the subtracted map is computed as

$$\rho_{(x,y)} = (n_{(x,y)}^{South} - n_{(x,y)}^{North}) / \sigma_{(x,y)}$$

where

$$\sigma_{(x,y)} = \sqrt{n_{(x,y)}^{South} + n_{(x,y)}^{North}} .$$

The derived map is presented in Fig. 11. The first point to note is that South-North overdensities larger than  $5\sigma$  are present essentially everywhere in the considered area, in agreement with the results discussed in previous sections. It is clear that this region of the Galaxy is pervaded by a global overdensity that declines with distance (mainly traced by blue and cyan regions), as expected from a structure due to a deformation of the Galactic Disc, i.e. the warp. On

top of this we see a strong and spatially confined overdensity, centred at  $(x,y)=(-3.6 \text{ kpc}, -6.2 \text{ kpc})$ , the Canis Major structure. The core of CMa appears as a deformed elliptical structure whose spatial orientation is the same as depicted in Fig. 7. This core is surrounded by a large lower-density halo that reaches  $(x,y)\sim(4.0 \text{ kpc}, -14.0 \text{ kpc})$ . This larger structure may be partly associated to the main body of CMa (approximately for  $x < 0 \text{ kpc}$ ) and partly associated with tidal structures of possibly unbound stars (tidal tails, for  $x > 0 \text{ kpc}$ , approximately). It is interesting to note that the small structure at  $(x,y)\sim(-10.0 \text{ kpc}, -10.0 \text{ kpc})$  corresponds to the anomaly around  $l \simeq 220^\circ$  noted in Fig. 5 and discussed in Sect. 4.1. Fig. 11 supports the view that this feature may be associated with an arm of the Ring lying behind the main body of CMa (see Fig. 7 and Pap-IV). The smaller features at  $(x,y)\sim(-5 \text{ kpc}, -13 \text{ kpc})$ ,  $(x,y)\sim(1 \text{ kpc}, -13.5 \text{ kpc})$  and, possibly,  $(x,y)\sim(5 \text{ kpc}, -14 \text{ kpc})$ , all lying approximately at the same  $r = \sqrt{x^2 + y^2}$ , may be other fragments of the same structure.

Note also that the perspective effects discussed in Sect. 4.1 can be more readily interpreted by examining Fig. 11. For instance, it is clear that going from  $l \sim 220^\circ - 240^\circ$  to  $l = 280^\circ$  (a) the density of the structures crossing the line of sight decreases with  $l$ , (b) the average distance to the densest parts of the structure increases with  $l$ , and (c) the line-of-sight width of the structure increases with  $l$ , up to  $l \sim 300^\circ$ . The effects of these *physical* features have been noted and discussed in Sect. 4 and Sect. 4.1.

Finally, it is worth recalling that, in contrast with the 2-D sky maps shown in Figs. 8 and 9, above, there is no model and no fit involved in the derivation of the map shown in Fig. 11. The map is the simple result of the subtraction of the southern and northern density maps as obtained from the data.

If the global smooth overdensity is related to the Galactic Disc it should be possible to subtract it from the map of Fig. 11. Since the overall number of southern RC stars in our sample is 1.2 times that found in the Northern hemisphere, as the simplest assumption we rescale the density of

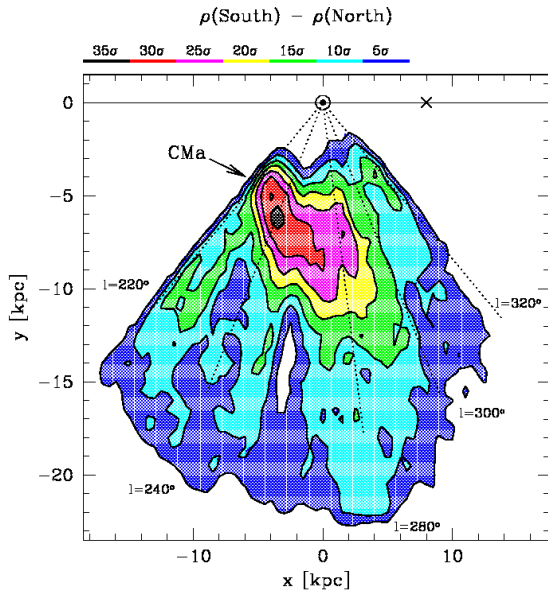


**Figure 11.** Maps of South-North residual density (in  $\sigma$  units) projected onto the Heliocentric  $x,y$  plane. The position of the Sun is marked by the usual circled-dot symbol, the  $\times$  symbol marks the position of the Galactic Centre. Note that the “hole” at  $(x,y)\sim(-3.0,-15.0)$  corresponds to a region where the overdensity is below the  $5\sigma$  threshold but still positive and  $\gtrsim 3\sigma$ . The paths of some remarkable lines of sights are reported as dotted lines, as a reference.

the Northern map by this factor and repeat the subtraction. The resulting map of residuals is shown in Fig. 12. Adopting a safe  $10\sigma$  cut, the only surviving structure is CMa, plus tiny traces of the  $(x,y)\sim(-10.0\text{ kpc}, -10.0\text{ kpc})$  feature. Note that large negative residuals appear only near the edges of the map. This means that the rescaled northern density map is a reasonable model of the large-scale overdensity observed in the southern hemisphere. We tried different simple models fitting the overall decline of density with  $r$ : in all cases the only overdensity surviving the subtraction of the model to the southern density map is CMa, in all cases displaying the characteristic shape shown in Figs. 11 and 12. This exercise strongly supports our interpretation of the southern overdensities in the considered region of the Galaxy in terms of a large-scale Galactic asymmetry (warp) plus a disrupting dwarf galaxy (CMa).

#### 4.4.1 The Argo structure

While the present paper was near completion a preprint was posted (Rocha-Pinto et al. 2005, hereafter RP05) studying the distribution of 2MASS M giants at low galactic latitudes ( $|b| \leq 20^\circ$ ). Adopting an extinction grid with a finer resolution compared to previous analyses of M-giants (Majewski et al. 2003; Crane et al. 2003, Pap-I), and using a starcounts model to subtract the smooth Galactic components, they are able to follow overdensities down to lower absolute latitudes ( $|b|$ ) than, for instance, in Pap-I. They find that, in the  $220^\circ \leq l \leq 320^\circ$  region studied here, all the existing overdensities are enclosed in the range of He-

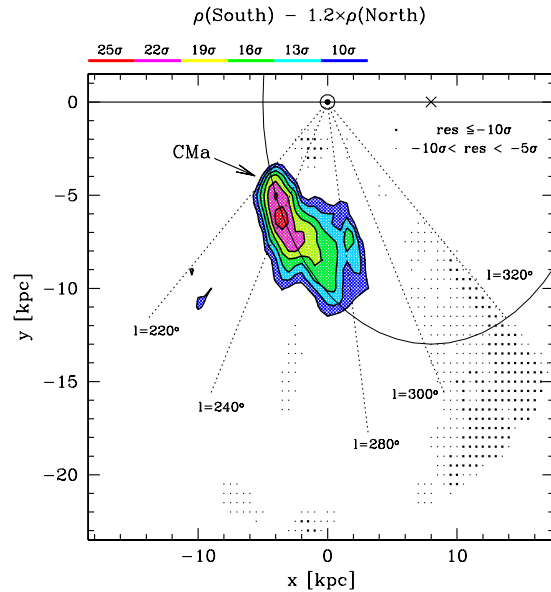


**Figure 12.** The same as Fig. 11 but with the Northern hemisphere density map rescaled by a factor 1.2. Note that essentially all the smooth component of the overdensity disappears, leaving the main body of CMa as the only positive residual. The paths of some useful lines of sights are reported as dotted lines, as a reference. Small dots mark positions of the grid where the residuals of the subtraction are  $-10\sigma < res < -5\sigma$ , large dots marks larger negative residuals ( $res \leq -10\sigma$ ). A circle centred on the Galactic centre with radius  $r = 13.0$  kpc is also shown as a visual guide.

liocentric distances  $6.0\text{ kpc} < D_\odot < 20\text{ kpc}$ . They confirm the presence of the CMa overdensity in this range but they claim that it is part of a larger and denser structure, centred around  $l \simeq 290^\circ$ , that they interpret as a large dwarf galaxy which they name *Argo*. They suggest that *Argo* and CMa can be erroneously seen as separated entities only because of a plume of extinction located at  $l \simeq 265^\circ$  extending to  $b \simeq -12^\circ$  (see Fig. 8) that introduces an artificial discontinuity in the surface density. Note that the main body of the claimed *Argo* structure is the elongated overdensity shown in the lower panel of Fig. 8 (compare with Fig. 1 and Fig. 3 of RP05), that we interpret as the region of maximum surface density of the Warp as seen from the Sun.

The results obtained in the present contribution do not support the analysis of RP05. Let us summarise the main arguments against their interpretation of the *same* overdensities studied here.

(i) R05 identify *Argo* as an overdensity enclosed in the range of distances  $6.0\text{ kpc} < D_\odot < 20\text{ kpc}$  and claim that its core (around  $l \sim 280^\circ - 290^\circ$  appears localised in distance. Pap-II (using M giants) and Figs. 3, 11 and 12 here (relying on RC stars) demonstrate that Canis Major is a much more spatially-confined structure than *Argo*. CMa spans the range  $5\text{ kpc} \lesssim D_{sun} \lesssim 13\text{ kpc}$  and this extent in distance is due to the orientation of the major axis, the actual minor-axis width spans less than 4 kpc across. The major axis of CMa is approximately oriented along the path of a nearly-circular orbit around the centre of the Galaxy (see Fig. 7 and

Fig. 12), consistent with the N-body simulation presented in Pap-IV.

(ii) The Argo structure emerges from integrating stars (M giants or RC stars) over a large range of distance ( $6.0 \text{ kpc} < D_{\odot} < 20 \text{ kpc}$ ). Fig. 3 and, above all, Figs. 11 and 12, show that there is no coherent 3-D structure corresponding to the surface density structure centred around  $l \sim 290^{\circ}$  shown in the lower panel of Fig. 8 and in R05.

(iii) To support the proposition that the core of Argo is spatially confined, RP05 present the subtracted CMD of a field centred at  $(l; b) = (285^{\circ}; -5^{\circ})$  in which the weak signal of a Red Clump can be perceived. Fig. 13, coupled with Figs. 11 and 12, explains the origin of this feature in the CMD. The figures display the SLF of selected  $5^{\circ} \times 5^{\circ}$  fields centred at  $b = -7.5^{\circ}$  and  $l = 245^{\circ}, 285^{\circ}$  and  $297.5^{\circ}$ . The l.o.s. sampled by the  $l = 245^{\circ}$  field (upper panel) crosses the core of CMa: the characteristic narrow RC bump is superposed on a weak exponential SLF. The l.o.s. sampled by the  $l = 285^{\circ}$  field should cross the centre of the putative Argo structure. The contribution of the UP (warp) to the SLF is much stronger here but an RC bump is still clearly visible, in agreement with what is shown in Fig. 5 and discussed in Sect. 4. However, the contribution of the bump to the overall SLF is lower than that provided by the UP, and the RC peak is much broader. A comparison with Figs. 11 and 12 shows that this l.o.s. is in fact crossing the wide low-density structure around  $(x, y) \sim (2 \text{ kpc}, -7.5 \text{ kpc})$  that spans  $\sim 8 \text{ kpc}$  along this l.o.s., and is probably associated with the tidal tail of CMa. The l.o.s. sampled by the  $l = 297.5^{\circ}$  field hits the outer limit of the CMa structure with an even less favourable orientation. Consequently the RC bump signal in the SLF is even weaker and a clear peak is not perceivable. In conclusion, the feature presented by RP05 as the RC of Argo is in fact a trace of the RC of the outer regions of CMa widely dispersed along the line of sight.

(iv) RP05 derive (from M giants) an estimate of the total luminosity of  $L = 3.7 - 15 \times 10^6 L_{\odot}$  for Argo. Limiting ourselves to the stars contributing to the map in the lower panel of Fig. 8 and in the range  $-20^{\circ} \leq b \leq 0^{\circ}$  and  $265^{\circ} \leq l \leq 320^{\circ}$  we count more than  $1.8 \times 10^6$  stars. With the assumptions stated in Sect. 3.2 we obtain  $L \sim 1.2 \times 10^9$ , orders of magnitude larger than the R05 estimate. Note that our estimate should be considered as a lower limit since (a) the contribution of CMa is not included, while RP05 consider it as a part of Argo, and (b) we limited the calculation to the approximate distance range  $5 \text{ kpc} \leq D_{sun} \leq 13 \text{ kpc}$ , while R05 integrate over  $6.0 \text{ kpc} < D_{\odot} < 20 \text{ kpc}$ . Hence the beautiful consistency among the luminosity estimates obtained from M-giants, RC stars and MS stars achieved for CMa (Sect. 3.2) is completely lost in the case of Argo. This strongly suggests that Argo is not a coherent stellar system, but is instead just a surface density structure that originates from the mix of different (and unrelated) populations that happen to lie along the same line of sight.

(v) RP05 discard the warp hypothesis for the nature of Argo claiming that the shape of the structure is not "warp-like". However, in their view, *all* the southern overdensities in the  $220^{\circ} \leq l \leq 320^{\circ}$  region are due to Argo and CMa. The implicit conclusion is that the Galactic Warp (and flare) does not produce any observable South-North asymmetry in this region, at odds with the conclusions of López-Corredoira et al. (2002). The smooth nature of the

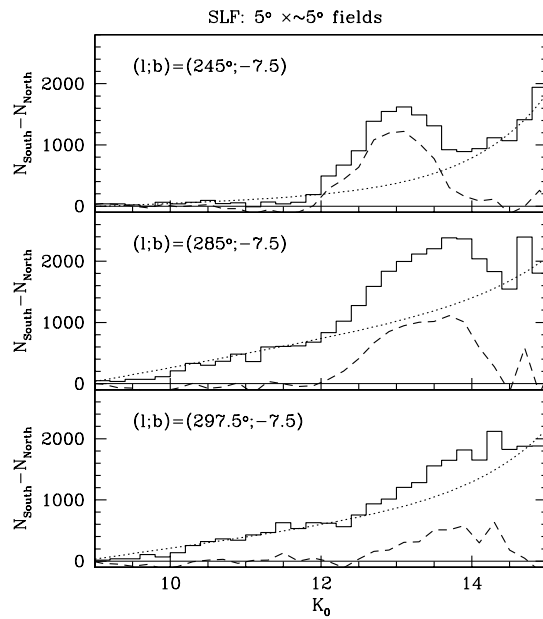


**Figure 13.** SLFs of  $5^{\circ} \times 5^{\circ}$  fields sampling, respectively: (a, upper panel) a line of sight crossing the core of CMa, (b, middle panel) a line of sight crossing the wide halo of CMa — see Fig. 12 — or the putative Argo centre, (c, lower panel) a line of sight passing outside the main CMa overdensity. The symbols are the same as in Figs. 2, 3, 4, and 5.

global South-North asymmetry shown to be present in this region, its Galactic-scale dimensions, and the fact that a rescaled version of Northern density map is a good model for it (Fig. 12), strongly indicate that the surface density structure centred around  $l = 290^{\circ}$  is not a dwarf galaxy remnant (Argo) but the effect of the Warp (and flare) asymmetries of the Galactic disc.

Finally, we recall again that the RC distance scale used here is much more reliable and accurate compared to the distance scale obtained from M giants. This allowed us to obtain the extremely clear maps shown in Figs. 11 and 12, where CMa appears as the strongest and the only structured overdensity in that region while we do not see any trace of Argo.

## 5 SUMMARY AND CONCLUSIONS

We have performed a differential analysis of the distribution of the Southern Galactic hemisphere excess of colour-selected Red Clump stars extracted from 2MASS in the region  $220^{\circ} \leq l \leq 320^{\circ}$  and  $-30^{\circ} \leq b \leq +30^{\circ}$ . Our main aim was to trace the structure of the main body of the newly discovered Canis Major stellar system (Pap-I) and of the stellar component of the southern part of the Galactic Warp (Pap-II, Pap-III). The focus on these structures and on their (possible) relation drove our decision to "limit" the analysis to the above-quoted range of Galactic latitudes. In each considered field located in the Southern galactic hemisphere we obtained the K Luminosity Function of RC stars and we subtracted from it the K Luminosity Function of RC stars of the Northern hemisphere field located at the symmetric posi-

tion with respect to the Galactic Plane. In these Subtracted Luminosity Functions (SLFs) the Canis Major RC population is easily identified (in the range  $220^\circ \lesssim l \lesssim 270^\circ$ ) as a significant and well-defined bump within  $11.5 \leq K \leq 14.0$ , placed on top of an exponential component that is present all over the considered magnitude range  $10.0 \lesssim K \lesssim 15.0$  and is detected everywhere between  $l = 220^\circ$  and  $l = 320^\circ$ , with a maximum in star counts around  $l \sim 290^\circ$ . We identify this latter large-scale South/North overdensity as due to the Galactic Warp. By fitting the exponential component of the SLFs we are able to partially disentangle the contribution of the two overdensities, so obtaining a quantitative description of the main body of CMa, fully independent of previous analyses, and a global picture of CMa and the Warp in this region of the sky.

The main results we have obtained can be summarised as follows:

- The Canis Major system is not related to the Galactic Warp. The latter gives rise to a South/North overdensity that (a) produces featureless SLFs, i.e. with no detectable bump, as expected from a structure that is quite extended along the line of sight, (b) it has a scale larger than the portion of sky considered in the present analysis (i.e. larger than  $100^\circ$ ), (c) it displays a number surface density (for sources with the same luminosity as CMa RC stars, i.e.  $11.5 \leq K \leq 14.0$ ) that is everywhere comparable or larger than what is observed at the centre of CMa, (d) it shows a very strong maximum around  $l = 290^\circ$  and  $b > -6^\circ$  in agreement with the results of López-Corredoira et al. (2002). Canis Major appears as a narrow and confined stellar system that is “superposed” on the Warp structure and is located in front of the largest portion of the Warp (see Fig. 3, for example). This view appears fully evident from the 3-D distributions displayed in Fig. 11 and Fig. 12.

- RC stars provide a quantitative description of CMa that is in full agreement with those obtained with other independent tracers (M giants and MS stars, see Pap-I, Pap-II, Pap-III and Martínez-Delgado et al. 2005). In particular we obtained a (distance-independent) estimate of the integrated V magnitude and a (distance-dependent) estimate of the central surface brightness in excellent agreement with those obtained by Martínez-Delgado et al. (2005) from deep optical photometry of MS stars. We also obtained a distance profile (along the line of sight) of CMa that is essentially indistinguishable from that obtained in Pap-III from M giants. The high degree of self-consistency achieved among the various analyses — using different tracers — may be considered also as a validation of our criterion of selection of RC stars. The fundamental parameters of the CMa system as derived in the present study are summarised in Table 3. We confirm, with independent tracers and an independent distance scale with respect to Pap-I and Pap-III, that the mean distance of CMa is  $D_\odot = 7.2 \pm 1.0$  kpc.

- We have detected a clear relation between the mean distance to CMa and Galactic longitude within the main body (see Table 1). The derived spatial orientation of the system is in good agreement with the predictions of the N-body simulation presented in Pap-IV, that models CMa as a dwarf galaxy being accreted in a planar orbit onto the disc of the Milky Way.
- Using the same dataset (2MASS), the same tracer (RC

**Table 3.** Fundamental parameters of the main body of the Canis Major system.

$\langle D_{sun} \rangle$	$7.2 \pm 1.0$ kpc
$\langle D_{sun} \rangle$ vs. $l$	see Tab. 1
$\langle l \rangle$	$248.1^\circ \pm 2.0^\circ$
$\langle b \rangle$	$-7.0^\circ \pm 0.3^\circ$
$\langle R_{GC} \rangle$ <sup>a</sup>	$12.6 \pm 1.0$ kpc
X	$-10.7 \pm 0.4$ kpc
Y	$-6.6 \pm 0.9$ kpc
Z	$-0.9 \pm 0.1$ kpc
$M_V$	$-14.1 \pm 0.9$ mag
$\mu_{V,0}$	$24.0 \pm 0.7$ mag/arcsec <sup>2</sup>
$HWHM_{l.o.s.}$	$\simeq 2.0$ kpc
$HWHM_l$ <sup>b</sup>	$\sim 15^\circ$
$HWHM_b$ <sup>c</sup>	$\sim 5^\circ$

<sup>a</sup> Assuming the above estimates of the position of the centroid of the system, and propagating the associated uncertainties. The same assumptions hold for the X, Y, Z galactocentric coordinates (see Fig. 7, for definitions).

<sup>b</sup> Indicative estimate from the maps of Fig. 8 and 9.

<sup>c</sup> Indicative estimate from the maps of Fig. 8 and 9.

stars) and the same distance scale as in the analysis summarised above, we showed that the old open clusters AM 2, To 2 and Haf 11 are located within the main body of Canis Major.

We also investigate the claim made in the recent study by Rocha-Pinto et al. (2005), that Canis Major is an external field of a larger Argo structure, which would be the true centre of the dwarf galaxy remnant accreted onto the Milky Way. The distribution of red clump stars along the line of sight does not support this conclusion, however. Unlike the situation in the Canis Major region, we find no significant peak along the line of sight through Argo that would indicate the presence of a localised structure. We conclude that Argo is most likely not related to Canis Major, and is probably an asymmetry of Galactic origin.

In summary, the present study fully (and independently) confirms the results presented in previous papers of this series and in Martínez-Delgado et al. (2005): Canis Major has the size, the luminosity and the kinematics typical of a large dwarf galaxy, seen during the last stages of its disruption within the tidal field of the Milky Way (see also Sbordone et al. 2005). While further details emerge — as, for example, the distance-longitude gradient — we begin to obtain a clearer view of this challenging system. Future studies should try to overcome the several observational challenges posed by this nearby, low latitude object, to unveil the details of its stellar content (age, chemical composition) and to clarify its possible connection with the Ring.

## ACKNOWLEDGMENTS

The financial support of ASI and MIUR is acknowledged. This publication makes use of data products from the Two Micron All Sky Survey, which is a joint project of the University of Massachusetts and the Infrared Processing and Analysis Center/California Institute of Technology, funded



by the National Aeronautics and Space Administration and the National Science Foundation. This research has made use of NASA's Astrophysics Data System Abstract Service. The assistance of P. Montegriffo in the development of the software required for the present analysis is also acknowledged.

## REFERENCES

- Abadi M.G., Navarro J.F., Steinmetz M., Eke V.R., 2003b, *ApJ*, 597, 21
- Abadi M.G., Navarro J.F., Steinmetz M., Eke V.R., 2003a, *ApJ*, 591, 499
- Babusiaux C., Gilmore G., *MNRAS*, in press (astro-ph/0501383)
- Bellazzini M., Ferraro F.R., Ibata R., 2002, *AJ*, 124, 915
- Bellazzini M., Ferraro F.R., Ibata R., 2003a, *AJ*, 125, 188
- Bellazzini M., Ibata R., Ferraro F.R., Testa V., 2003b, *A&A*, 405, 577
- Bellazzini M., Ibata R., Ferraro F.R., 2003c, in *Satellites and Tidal Tails*, D. Martinez-Delgado and F. Prada Eds., S. Francisco, ASP, ASP Conf. Series, Vol. 327, in press (astro-ph/0304502)
- Bellazzini M., Ibata R., Monaco L., Martin N., Irwin M.J., Lewis G.F., 2004, *MNRAS*, 354, 1263 (Pap-II)
- Binney J., 1992, *ARAA*, 30,51
- Bonifacio P., Monai S., Beers T.C., 2000, *AJ*, 120, 2065
- Brown J.A., Wallerstein G., Geisler D., Oke J.B., 1996, *AJ*, 112, 1551
- Cole, A.A., 2001, *ApJ*, 559, L17
- Crane J.D., Majewski S.R., Rocha-Pinto H., Frinchaboy P.M., Skrutskie M.F., Law R.D., 2003, *ApJ*, 594, L119
- Cutri et al., 2003, Explanatory Supplement to the 2MASS All Sky Data Release, <http://www.ipac.caltech.edu/2mass/releases/allsky/doc/explsup.html>
- Djorgovski S., Sosin C., 1989, *ApJ*, 341, L13
- Forbes D.A., Strader J., Brodie J.P., 2004, *AJ*, 127, 3394
- Frinchaboy P.M., et al., 2004, *ApJ*, 602, L21
- Helmi A., 2004, *ApJ*, 610, L97
- Helmi A., White S.D.M., Springel V., 2003, *MNRAS*, 339, 834
- Helmi A., Navarro J., Meza A, Steinmetz M., Eke V., 2003, *ApJ*, 592, L25
- Ibata, R.A., Irwin, M.J., Gilmore, G., 1994, *Nature*, 370, 194
- Ibata, R.A., Wyse, R.F.G., Gilmore, G., Irwin, M.J., & Suntzeff, N.B., 1997, *AJ*, 113, 634
- Ibata R., Lewis G., 1998, *ApJ*, 500, 575
- Ibata R., Lewis G., Irwin M., Totten E., Quinn T., 2001, *ApJ*, 551, 294
- Ibata R., Lewis G., Irwin M., Cambrésy L., 2002, *MNRAS*, 332, 921
- Ibata R., Irwin M., Lewis G., Ferguson A., Tanvir N., 2003, *MNRAS*, 340, L21
- Ivanov V.D., Borissova J., Pessev P., Ivanov G.R., Kurtev R., 2002, *A&A*, 394,1
- Ivezic, Z., et al., 2000, *AJ*, 120, 963
- Johnston K., Sackett P.D., Bullock J.S., 2001, *ApJ*, 557, 137
- Johnston K.V., Law D.R., Majewski S.R., 2005, *ApJ*, 619, 800
- Kinman T.D., Saha A., Pier J.R., 2004, *ApJ*, 605, L25
- Kubiak M., Kaluzny J., Krzemiński W., Mateo M., 1992, *Acta Astronomica*, 42, 155
- Kuijken K., Garcia-Ruiz I., 2001, in *Galaxy Disks and Disk Galaxies*, J.G. Funes, S. J. and Enrico Maria Corsini Eds., San Francisco: ASP, ASP Conf. Series, Vol. 230, 401
- López-Corredoira M., Cabrera-Lavers A., Garzón F., Hamersley P.L., 2002, *A&A*, 394, 883
- Law D.R., Johnston K.V., Majewski S.R., 2005, *ApJ*, 619, 807
- Majewski S., Skrutskie M., Weinberg M., Ostheimer J., 2003, *ApJ*, 599, 1082
- Maraston C., 1998, *MNRAS*, 300, 872
- Maraston C., 2005, *MNRAS*, submitted (astro-ph/0410207)
- Martin N., Ibata R.A., Bellazzini M., Irwin M.J., Lewis G.F., Dehnen W., 2004a, *MNRAS*, 348, 12 (Pap-I)
- Martin N., Ibata R.A., Bellazzini M., Conn B., Irwin M.J., Lewis G.F., McConnachie A.W., 2004b, *MNRAS*, 355, L33 (Pap-III)
- Martin N., Ibata R.A., Conn B., Lewis G.F., Bellazzini M., Irwin M.J., 2005, *MNRAS*, submitted
- Martinez-Delgado D., Butler D.J., Rix H.-W., I. Franco, J. Penarrubia, 2005, *ApJ*, submitted (astro-ph/0410611)
- Mateo M., 1998, *ARA&A*, 36, 435
- Mateo C.E., Vivas A.K., Zinn R., Miller L., 2005, in *International Workshop Astronomia Dinamica en Latino-America (ADeLA 2004)*, C. Abad, A. Bongiovanni and Y. Guillen Eds., Rev. Mex. A.A. Conf Ser., in press (astro-ph/0504333)
- Mermilliod J.-C., 1995, in *Information and On-Line Data in Astronomy*, D. Egret and M.A. Albrecht Eds., Dordrecht, Kluwer, 127
- Monaco, L., Bellazzini, M., Ferraro, F.R., Pancino, E., 2003, *ApJ*, 597, L25
- Monaco, L., Bellazzini, M., Ferraro, F.R., Pancino, E., 2004, 353, 874
- Momany Y., Zaggia S.R., Bonifacio P., Piotto G., De Angeli F., Bedin L.R., Carraro G., 2004, *A&A*, 421, L29 [M04]
- Morrison H.L., Mateo M., Olszewski E.W., et al., 2000, *AJ*, 119, 2254
- Newberg H., et al. 2002, *ApJ*, 569, 245
- Newberg H., et al. 2003, *ApJ*, 596, L191
- Ortolani S., Bica E., Barbuy B., 1995, *A&A*, 300, 726
- Paczynski B., Stanek K., 1998, *ApJ*, L219
- Penarrubia J., Martinez-Delgado D., Rix H.-W., et al., 2005, *ApJ*, submitted, (astro-ph/0410448)
- Pietrinferni A., Cassisi S., Salaris M., Castelli F., 2004, *ApJ*, 612, 168
- Renzini A., 1998, *AJ*, 115, 2459
- Renzini A., Buzzoni A., 1986, in *Spectral evolution of galaxies*, C. Chiosi and A. Renzini Eds., Dordrecht, Reidel, p. 135
- Renzini A., Fusi Pecci F., 1988, *ARAA*, 26, 1999
- Rieke G.H, Lebofsky M.J., 1985, *ApJ*, 290, 116
- Robertson B., Bullock J.S., Font A.S, Johnston K.V., Hernquist L., 2005, *ApJ*, submitted (astro-ph/0501398)
- Robin A.C., Reylé S., Derrière S., Picaud S., 2003, *A&A*, 409, 523 [R03]
- Rocha-Pinto H., Majewski S., Skrutskie M., Crane J., 2003, *ApJ*, 594, L115
- Rocha-Pinto H., Majewski S., Skrutskie M., Patterson R.J.,

- 2005, ApJ L, submitted (astro-ph/0504122)  
Salaris M., Girardi L., 2002, MNRAS, 337, 332  
Sarajedini A., Grochlski A.J., Levine J., Lada E., 2002, AJ, 124, 2625  
Sbordone L., Bonifacio P., Marconi G., Zaggia S., Buonanno R., 2005, A&A, 430, L13  
Schlegel D., Finkbeiner D., Davis M., 1998, ApJ 500, 525 (SFD98)  
Vig S., Ghosh S.K., Ojha D.K., 2005, A&A, in press (astro-ph/0503388)  
White S., Rees M., 1978, MNRAS, 183, 341  
White S., Frenk C., 1991, ApJ, 379, 52  
Yanny B., et al. 2003, ApJ 588, 824  
Yusifov I., 2004, in The Magnetized Interstellar Medium, B. Uyaniker, W. Reich & R. Wielebinski Eds., in press (astro-ph/0405517)